COMBUSTION SYNTHESIS AND DOPING OF TITANIUM DIOXIDE

by

WALTER ALEXANDER MORALES

Presented to the Faculty of the Graduate School of

The University of Texas at Arlington in Partial Fulfillment

of the Requirements

for the Degree of

MASTER OF SCIENCE IN CHEMISTRY

THE UNIVERSITY OF TEXAS AT ARLINGTON

August 2007

World like a dewdrop

though it's only a dewdrop

even so, even so.

ISSA (1763-1827)

ACKNOWLEDGEMENTS

I would like to gratefully acknowledge my Supervisor, Dr. Krishnan Rajeshwar, for his enthusiastic inspiration, common-sense, vast knowledge and his great effort to explain things clearly and simply. I could not have imagined having a better advisor and mentor.

It was wonderful to be part of the team at the Electrochemistry Research Laboratory. This work would not have been possible without the support and encouragement of Dr. C. R. Chenthamarakshan, who has been abundantly helpful. Thanks also to Dr. N. R. de Tacconi for her assistance all these years. I express my gratitude to my colleges for their support, interest and valuable hints (Apichon, Wilaiwan, Marly, Hari, Yogee and Samanthi). We all make a great team of people motivated by science and innovation.

I would also like to thank my friends, for being the surrogate family during these years. Specially Mauro, whose passion for science always inspired me.

To my family that even from the distance always believed in me. My parents, specially, who encouraged me to pursue my dreams.

Finally, my special thanks to my wife Monica, whose love enabled me to complete this work and kept me going during hard times. You are truly the most amazing gift I have.

July 30, 2007

ABSTRACT

COMBUSTION SYNTHESIS AND DOPING OF TITANIUM DIOXIDE

Publication No. _____

WALTER ALEXANDER MORALES, M.S.

The University of Texas at Arlington, 2007

Supervising Professor: Krishnan Rajeshwar

A novel combustion technique was used for the preparation and doping of titanium dioxide (TiO_2). This metal oxide of titanium is a large band gap semiconductor (3.0 - 3.2 eV) that primarily absorbs in the ultraviolet region of the electromagnetic spectrum. However, the combustion synthesized TiO_2 ($CS-TiO_2$) prepared here, presented a shift in the absorption of light to the visible region of the spectrum and a high photocatalytic activity toward the reduction of $Cr(VI)$. The final product was characterized using X-ray powder diffraction (XRD), diffuse reflectance spectroscopy, X-ray photoelectron spectroscopy (XPS) and scanning electron microscopy (SEM). Comparison to a commercial TiO_2 (P-25 from Degussa) benchmark sample was used in each case. Diffuse reflectance spectroscopy showed an optical bandgap as low as 2.5 eV in the case of cationic doping with sulfur (present as a mixture of 4+ and 6+ states) and 1.7 eV in the case of co-doping with molybdenum. XPS studies showed doping and co-doping of the host oxide in each case precluding possible doping by carbon or nitrogen. An increase in the photocatalytic activity of this semiconductor toward the reduction of hexavalent chromium under visible light was achieved. Combustion synthesis opens up a wide range

of synthetic possibilities of oxide semiconductors because of its low energy requirement and simplicity.

TABLE OF CONTENTS

LIST OF FIGURES

LIST OF TABLES

CHAPTER 1

INTRODUCTION

1.1 Overview

As part of the growing awareness and concern about a sustainable planet, a big effort has been directed to green practices and environmental remediation in the industry and human activities in general. Several methods and approaches have been used to accomplish this task, and one of the most promising is heterogeneous photocatalysis using semiconductor nanoparticles [1-6].

Large band gap oxide semiconductor materials (TiO_2, WO_3, ZnO, CdS) for photocatalysis show advantages such as stability (chemical inertness and photostability), non-toxicity and low cost. In addition, many of these materials exhibit catalytic activity after repeated photocatalytic cycles and can be recovered using physical methods once the reaction is completed without significant loses [4]. These advantages make semiconductor photocatalysis a real and promising method in attaining the goal for a clean and better environment. However, one of the disadvantages in the use of these materials is that ultraviolet (UV) light is required for photoexitation with attendant electrical energy costs [2, 3].

Among the materials used in heterogeneous photocatalysis, titanium dioxide (TiO_2) has been extensively used. While very robust and stable under irradiation, a major limitation of this material is its wide band gap (3.2 eV), such that the photoexcitation process requires light in the UV region of the electromagnetic spectrum. Furthermore, a high recombination rate of the photogenetated charge carriers (electrons and holes) makes the photocatalytic process inefficient. To make effective use of solar energy, a

photocatalyst should have low band gap energy or a mechanism to extend the light absorption to the visible region. Several approaches have been used to address this issue, e.g., dye sensitization and doping of the metal oxide with different ions and metals [7].

This work uses a novel synthesis technique to improve the photocatalytic activity of titanium dioxide TiO_2 under visible light irradiation. Combustion synthesis also takes advantage of the positive effect of doping on the opto-electronic attributes of the host oxide material.

1.2 Heterogeneous Photocatalysis

A heterogeneous photocatalytic reaction is defined as a catalytic process using a semiconductor material that, after illumination with light of suitable energy, generates charge carriers (electrons and holes). These photogenerated charge carriers can react with molecules or ions either in the bulk solution or adsorbed on the semiconductor surface. Otherwise, they can also intervene in fast recombination and emission of thermal energy. The last process is one of several competing effects which might limit the effectiveness of the photocatalytic process leading to low photoactivity [3]. This is a *heterogeneous* process because the catalyst (semiconductor) and the target for catalysis (molecules or ions in solution) are in two different phases, unlike in the *homogeneous* process counterpart.

1.2.1 Band Structure of Semiconductors and Band Gap Energy

When considering few atoms, it will be found that electrons occupy only specific orbitals or energy levels separated by forbidden energy gaps. However, when the number of bonded atoms increases, the energy levels become continuous, rather than being discrete. Thus, the valence orbitals form an energy *band* with discrete energy levels infinitesimally separated leading to the valence band (VB). A second band at a higher level of energy is referred to as the conduction band (CB). Finally, separating the two bands a forbidden

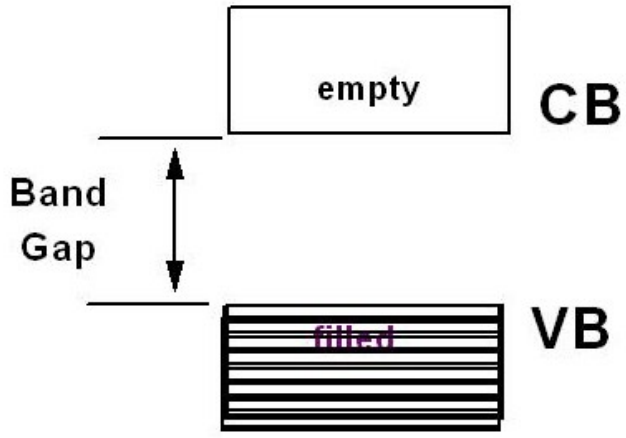

Figure 1.1. Schematic representation of a semiconductor showing the band gap.

energy region is established, where no electrons are allowed, which is called the band gap (E_g). Figure 1.1 shows these concepts as well as the position of energy levels to be occupied by electrons and holes, generated when an optical excitation occurs.

Based on these bands and the gap between them, metallic, insulator and semiconductor materials can be differentiated, thus identifying their electronic conductivity. Metallic materials have partially filled energy bands allowing electronic conduction. Insulators have a large separation of the bands, usually a value greater than 5 eV, and therefore conduction is not feasible. Figure 1.2 shows this concept together with representations of bands and the band gap for the three different types of materials. Notice the overlapping of conducting and valence bands in the case of metals.

Semiconductors have electronic properties in between those of metals and insulators. Their valence band is full while the conduction band is empty under normal conditions (just like an insulator)(see Figure 1.1). By increase of temperature or by photoexcitation, an electron can be promoted from the valence band to the conducting band. Therefore, an increase in conductivity occurs due to the free flow of the new charges in the previously empty band. If this is the case, then conductivity in these materials is an

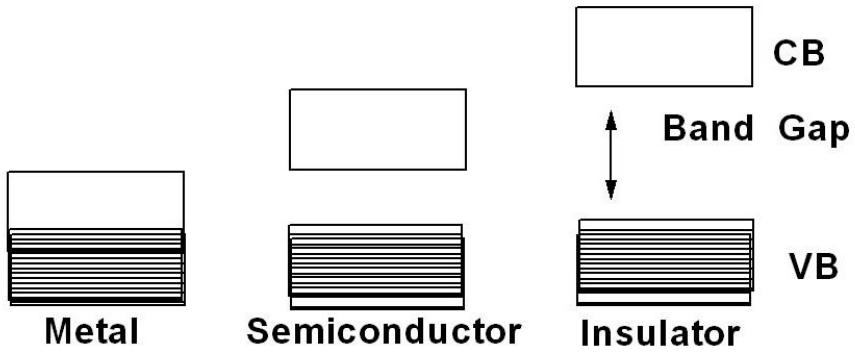

Figure 1.2. Energy band structures for metal, semiconductor and insulator materials.

inherent property and they are called intrinsic semiconductors. There is a second group of materials called extrinsic semiconductors, which are formed when conduction arises from doping with "impurities" in the host matrix.

1.3 Chemical Modification

Modifying the chemistry of a semiconductor can surmount limitations of such material as a photocatalyst. To date, three different types of modifications to photocatalytic semiconductor systems have been studied: inhibition of recombination by increasing the charge separation; increasing the wavelength response range (shift to visible light) and changing the selectivity or yield of a particular product [1, 7]. An example of the first type of modification involves addition of noble metals to the semiconductor to change the surface and suppress carrier recombination [1]. Thus the activity of a semiconductor photocatalyst such as TiO_2 is enhanced by the addition of small amounts of Pt and Ag [8]. The two remaining categories, which include spectral sensitization and doping will be discussed in sections 1.5.3.1 and 1.5.3.2.

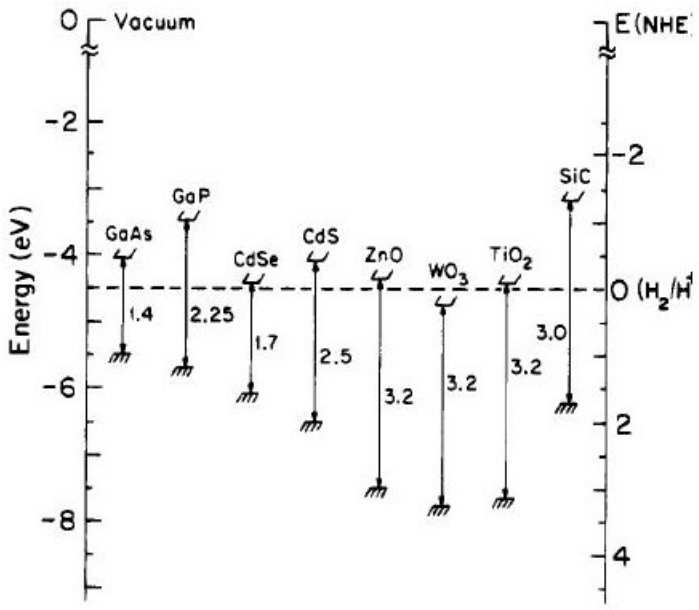

Figure 1.3. Band edge positions and band gap energies for some semiconductors [1].

1.4 Choice of Semiconductor Photocatalyst

Some special criteria have to be met in the choice of the semiconductor for a particular reaction. First, the standard reduction potential of the acceptor species must be more positive than the potential of the conduction band edge of the semiconductor surface in order to let the reduction reaction by the CB electrons to occur. On the other hand, to begin an oxidation process by the VB holes, the standard reduction potential of the donor must be more negative than the potential corresponding to the valence band edge of the semiconductor surface.

A comparison between the band edge positions of some semiconductors versus the standard hydrogen electrode (SHE) is illustrated in Figure 1.3, as well as the band gap energies of these materials.

1.5 TiO_2

Titanium dioxide, also known as titania, is an important commercial product that has been used in various commercial applications that range from industrial (paint and pigment), to cosmetic (skin-care products). On a research level, this material has attracted interest for water splitting [9], solar photovoltaic cells and water or air remediation [1, 5, 6, 10, 11]. This metal oxide has been used as a potential photocatalyst of choice for the total destruction (mineralization) of organic pollutants in air and water. As mentioned earlier, this semiconductor material has high activity and stability to light illumination, and also has non-toxic and widely occurring component elements [6, 10].

1.5.1 Properties of TiO_2

Titanium dioxide can exist in three bulk crystalline forms: rutile, anatase, and brookite. However, only rutile and anatase have seen applications in photocatalysis. Moreover, out of these two, anatase shows a higher photocatalytic activity [12]. The unit cell shown in Figure 1.4 represents their basic building blocks [10]. A central titanium atom is surrounded by six oxygen atoms in a distorted octahedral configuration for both rutile and anatase crystal structures. Furthermore, rutile exhibits an orthorhombic structure with a slight distortion while anatase shows a more significant distortion resulting in less orthorhombic symmetry. Figure 1.5 displays the different crystallographic parameters for the two phases of TiO_2 [12].

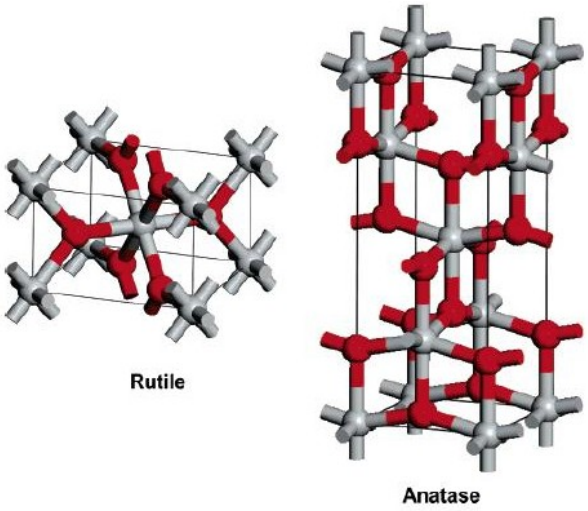

Figure 1.4. Unit cell for anatase and rutile phase of TiO_2, titanium is represented in grey and oxygen in red color [10].

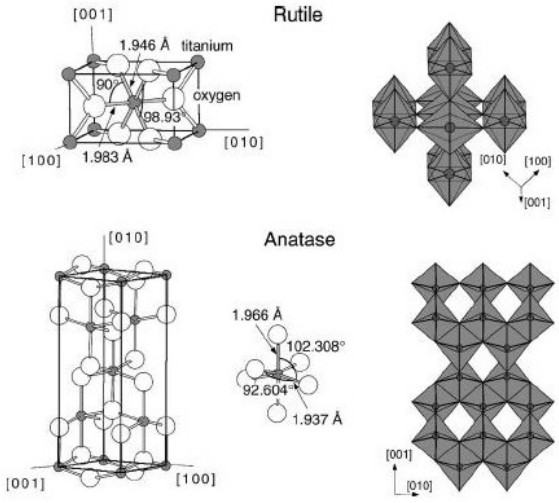

Figure 1.5. Different crystallographic parameters for the two main phases of TiO_2 [12].

For the different bond distances between atoms in the structure, the $Ti - Ti$ distances are greater in anatase than in rutile (3.79 - 3.04 $\mathring{A}$ vs. 3.57 - 2.96 $\mathring{A}$ respectively), whereas the $Ti - O$ distances are shorter for anatase (1.934 and 1.980 $\mathring{A}$ in anatase vs. 1.949 and 1.980 $\mathring{A}$ in rutile). In the rutile structure, each octahedron is in contact with 10 neighbor octahedrons (two sharing edge oxygen pairs and eight sharing corner oxygen atoms), while in the anatase structure, each octahedron is in contact with eight neighbors (four sharing an edge and four sharing a corner). These differences in lattice structures cause different physical properties e.g., mass density and electronic characteristics (e.g., band gaps). Thus the band gap threshold is 3.05 eV for rutile compared to 3.25 eV for anatase.

1.5.2 TiO_2 Photocatalysis

Titanium dioxide is a wide band gap semiconductor with a band gap of $\approx 3.0 - 3.2\, eV$. The valence band (VB) of TiO_2 is made of $O\ 2p$ orbitals, and the empty conduction band (CB) is derived from $Ti\ d$ orbitals; this constitutes the energy band structure of this semiconductor. In order for light to be absorbed, its wavelength should correspond to wavelengths shorter than $\approx 407nm$ for rutile and $\approx 382nm$ for anatase. Thus, upon photoexcitation of TiO_2, electrons (e^-) are promoted from the valence band (VB) to the conducting band (CB), leaving behind a positive charge generated for each electron promoted in the VB, which is called a hole (h^+). The fate of these two photogenerated charge carriers depends on the presence of electron or hole scavengers or surface defect states. As a result, the recombination process is avoided and the photocatalytic reaction can take place [3]. Several successive steps can be visualized as shown in Figure 1.6.

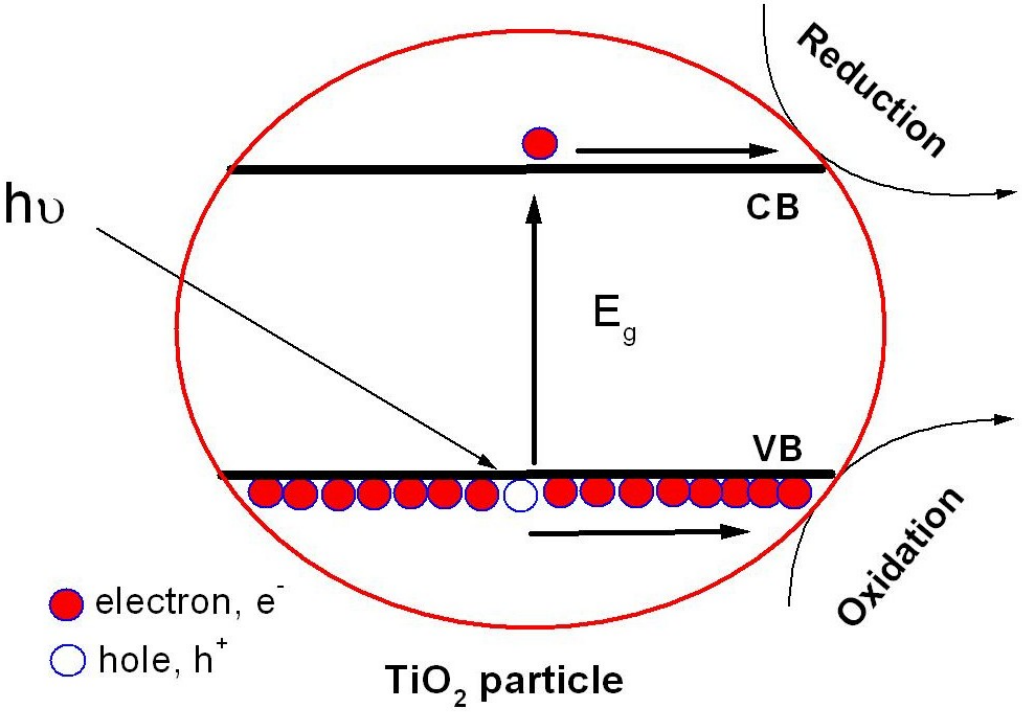

Figure 1.6. Schematic events in the bulk and surface of TiO_2.

The various events during heterogeneous photocatalysis can also be illustrated using equations [3] which are presented below. The first step is the charge carrier generation:

$$TiO_2 + h\nu \rightarrow h^+_{VB} + e^-_{CB} \tag{1.1}$$

After photogeneration, these charge carriers can be trapped at the surface:

$$h^+_{VB} + > Ti^{IV}OH \rightarrow \{> Ti^{IV}OH^{\bullet}\}^+ \tag{1.2}$$

$$e^-_{CB} + Ti^{IV}OH \leftrightarrow \{> Ti^{III}OH\} \tag{1.3}$$

$$e^-_{CB} + > Ti^{IV} \rightarrow > Ti^{III} \tag{1.4}$$

An alternative fate for the charge carriers is recombination:

$$h^+_{VB} + \{> Ti^{III}OH\} \rightarrow > Ti^{IV}OH \tag{1.5}$$

$$e^-_{CB} + \{> Ti^{IV}OH^{\bullet}\}^+ \rightarrow > Ti^{IV}OH \tag{1.6}$$

Finally, some of the charge carriers are transferred from the semiconductor to adsorbed or solution species:

$$\{> Ti^{IV}OH^{\bullet}\}^+ + Red \rightarrow > Ti^{IV}OH + Red^{\bullet +} \tag{1.7}$$

$$e^-_{tr} + Ox \rightarrow > Ti^{IV}OH + Ox^- \tag{1.8}$$

In these equations $>TiOH$ represents the primary hydrated surface functionality of TiO_2, e^-_{CB} represents an electron in the conduction band, e^-_{tr} is a trapped conduction-band electron and h^+_{VB} is a valence-band hole. Red and Ox represent the electron donor (i.e., reductant) and the electron acceptor (i.e., oxidant). $\{> Ti^{IV}OH^{\bullet}\}^+$ is the surface-trapped hole in the valence band (i.e., surface-bound hydroxyl radical), and $> Ti^{III}OH$ is the surface-trapped (CB) electrons [3].

Some key conclusions can be reached from a simple analysis of the above scheme: First, surface hydroxylation plays an important role in the initial phase of photocatalysis; second, surface hydroxyl radicals are the key oxidant species. These observations have been confirmed experimentally, showing that the surface density of OH-groups influences the photoactivity of TiO_2, as well as size of particle, surface area, anatase-rutile composition, and the presence of e^-/h^+ scavengers [3].

1.5.3 Methods for Improving Titania

Due to the relatively large band gap of TiO_2 (see above), UV light must be used in its photoexitation process, allowing with this the use of only 5% of the solar light that reaches the surface of the earth each day. Because of this, a great deal of research has focused on lowering the threshold energy for the photoexcitation process. As a consequence, a larger fraction of the solar spectrum could be used effectively for photocatalysis and other processes. Thus, the development of a photocatalytic TiO_2 system capable of

using natural sunlight to degrade organic and inorganic contaminants in wastewater can be achieved. These improvements in the overall performance of titania have been led by two main lines of research: dye sensitization and doping [7].

1.5.3.1 Dye sensitization

Dyes are natural light absorbers and electron transfer agents. They have been used for energy conversion in a process that copies the plant photosynthesis mechanism in electrochemical energy converting solar cells [11]. Dye sensitization is a process occurring when a light-excited dye molecule adsorbed at the semiconductor surface injects electrons into the conduction band of the semiconductor substrate. Titania based dye sensitization has potentially low cost, low environmental impact, and good power conversion efficiency. However, its more general use is limited by low quantum efficiency, high carrier recombination, low adsorption of the dye to the surface of the semiconductor material, dye desorption from the TiO_2 due to solvent effects, lack of long-term stability of the dye under light and heat, etc [1, 13].

1.5.3.2 Doping

There has been significant interest recently on both non-metal and transition metal doping of titanium dioxide TiO_2. The use of the so-called "impurities" creates extrinsic properties in the oxide host and a decrease in the band gap energy. The consequence is an increase in photoactivity under *visible* light irradiation. Different types of doping are reported for titania [1, 3], and due to the importance it represents in the present work, doping with nitrogen, carbon, sulfur and metal ions will be addressed separately in the following sections.

1.5.3.3 Nitrogen Doping

The idea of doping of titanium dioxide materials with nitrogen and other anionic species was presented in 2001 [14]. This report shows theoretical results for the substitution of C, N, F, P, or S atoms for oxygen atoms in the titania lattice. The study of density of states (DOS) for anatase TiO_2, suggests that substitutional doping using nitrogen is the most effective due to the mixing of nitrogen $2p$ states with oxygen $2p$ states, thus causing a significant decrease in the width of the overall band gap [14]. The theoretical predictions presented in the report were supported by experimental results using visible light and photooxidation tests for nitrogen doped TiO_2.

Using density functional theory (DFT) calculations, it was predicted that substitutional nitrogen doping results in a decrease in the band gap for the anatase phase, while the opposite effect was calculated for rutile TiO_2 [15]. This was attributed to the contraction of the valence band and stabilization of the $N\,2p$ state [15]. Experimentally, the same effect was found for the anatase phase [16-19]. Evidence for this type of doping was also established using XPS studies, and it was concluded that the nitrogen species responsible for the overall band gap narrowing effect had a binding energy value around 396 eV [14].

1.5.3.4 Carbon Doping

Studies on carbon dopants in TiO_2 using DFT calculations in anatase and rutile show that carbon impurities result in small variations of the band gap. Moreover, a creation of occupied states in the gap and formation of oxygen vacancies in bulk TiO_2 were reported [20]. The small variation in the band gap was also attributed to the position of doping in the gap, which was too deep to satisfy conditions of energy level

overlap [14]. Likewise, experimental reports show values of band gap as low as 2.32 eV for rutile and more efficient water splitting ability [21].

1.5.3.5 Sulfur Doping

Substitutional doping of sulfur similar to that of nitrogen doping has been reported [14]. However, sulfur doping was dismissed experimentally due to its large ionic size [14]. The idea was that substitution of sulfur at the oxygen sites could significantly modify the electronic structure of TiO_2, but conventional doping techniques could not achieve this because sulfur has a larger ionic radius compared to N or F [14]. Furthermore, narrowing effect and delocalization of the valence band edge is expected to occur only in the case of higher sulfur doping levels [19]. Experimentally, S-doped anatase TiO_2 has been obtained by oxidative heating of TiS_2 powder [22, 23], ion implantation, and thermal annealing [23]. These reports consider sulfur atoms occupying oxygen sites and forming Ti-S bonds. Mechanochemical doping using $Ti(OH)_4$ and thiourea with planetary ball mill followed by calcination, show titania with anatase and rutile compositions. XPS analyses gave binding energies around 168 - 169 eV that are assignable to sulfur as S^{6+} and S^{4+} [24]. Also, reports showed that doping with sulfur as S^{6+} and mixtures of the two oxidation states was achieved by mixing titanium isopropoxide with thiourea in ethanol, followed by evaporation and calcination in air [25, 26].

1.5.3.6 Doping with Transition Metals

Although the effect of metal doping of TiO_2 has been very widely studied with an intent to improve its catalytic activity, ambiguous conclusions are still often found. Some authors postulated that doping with cations having a valence higher than +4 can increase the photoactivity [27] while doping with trivalent metal ions would show a detrimental effect in photocatalytic activity [28]. However, an inconsistent mix of positive

and negative effects have been reported for the photocatalytic activity of doped TiO_2. For example, doping using Fe^{3+}, Mo^{5+}, Ru^{3+}, Os^{3+}, Re^{5+}, V^{4+}, and Rh^{3+} was claimed to increase the photoreactivity for oxidation and reduction processes [29]. However, the same study reported the opposite effect with Co^{3+} and Al^{3+} showing a decrease in photoreactivity [29]. Similar effects were found with low valence ($Fe^{3+}, Co^{2+}, Ni^{2+}$) and high valence cations (Mo^{5+}, Nb^{5+}, W^{6+}) [30]. Theoretically, the addition of Ti^{3+}, V^{3+}, Cr^{3+}, Mn^{3+}, and Fe^{3+} in both anatase and rutile TiO_2 crystal modifications were studied and it was concluded that there is a significant band gap narrowing effect for anatase; whereas, for the rutile modification no effect is expected [31].

The positive effect of metal doping is believed to be related to the energy level and d-electron configuration of the dopants in the host structure [29]. Additionally, it is believed that the presence of metal species allows the formation of a permanent space charge region on the surface of the semiconductor, improving the separation of photocarriers. Other authors conclude that although metal ion doping should decrease the photothreshold energy of TiO_2, the metal ion may also serve as a recombination center for electrons and holes, thus diminishing the overall activity of the photocatalyst [30, 32]. In conclusion, at present there is still no consensus in this matter and more research is needed in order to resolve the conflicting doping effects reported [32].

1.5.4 Methods for Preparation of TiO_2

While diffent methods have been used for the preparation of ceramic oxides and inorganic materials in general, most commonly solid-state synthetic rutes are used. However, these routes are time consuming and have high energy requirements [33]. Thus a search for more energy efficient methods in the preparation and improvement of oxide materials is relevant.

In the case of titania, industrial production makes use of the ilmenite mineral through the sulfate and chloride methods. The sulfate process starts with dissolving the ilmenite material in sulfuric acid to produce titanium oxysulfate ($TiOSO_4$). This is followed by neutralization with a base to yield hydrated titanium oxide. Finally, calcination produces the anatase or rutile product [34]. The hydrated oxide ($TiO_2.nH_2O$) and the product after calcination usually have low or no photocatalytic activity due to the presence of crystal defects and contaminants (normally Fe and S that remain from the reaction) [34]. The chloride method is quite similar to the sulfate route, but instead of sulfuric acid, chlorine gas at high temperature (1000-1300 K) is used. The product of this reaction, titanium tetrachloride ($TiCl_4$) is subjected to thermal decomposition to produce anatase or rutile [35]:

$$TiCl_{4(g)} + O_{2(g)} \rightarrow \ TiO_{2(S)} + 2Cl_{2(g)} \tag{1.9}$$

A large number of methods is emerging as synthetic routes for the preparation and doping of titania. These include: electrochemical methods [36, 37], ionized cluster beam deposition [38], aerosol process [39, 40], gas condensation [41], homogeneous precipitation at low temperatures [HPPLT][42], sol-gel process [43], mechanochemical synthesis [44], hydrothermal process [45-47] and combustion synthesis [33, 48, 49-51]. Comparatively, each method has advantages and disadvantages. For instance, aerosol process gives a pure product with no multiple steps, but the high temperature required leads to aggregation of particles. Among low temperature methods, the hydrothermal approach is attractive because of the use of $TiOSO_4$ as raw material and the use of a low temperature ($300\,^oC$) in aqueous media. However, the total time required varies between 1-6 hours and post preparation annealing of samples is required (temperatures higher than $450\,^oC$). Sol-gel process is also a low temperature method, but it incorporates a series of successive steps and costly chemicals and does not easily allow for control of composition. In addition,

the sample must be annealed in order to improve the photocatalytic activity [43]. On the other hand, combustion synthesis exhibits advantages over the other methods for the preparation of TiO_2. Because of the relevance of this particular method for this work, it is elaborated separately in the next section.

1.6 Combustion Synthesis

Combustion synthesis, also known as self-propagating high-temperature synthesis (SHS), uses a highly exothermic redox chemical reaction between metals and nonmetals, for the synthesis of oxide and nonoxide materials [33]. This method presents a variety of advantages that include: low energy requirement, generation of high-reaction temperature, short duration of reaction, high yields, highly crystalline products, simplicity and low cost [48, 52]. The synthesis is obtained through an exothermic, rapid, self-sustaining and self-propagating reaction. This is possible due to the large amount of heat released by the reaction itself, and is this exothermicity what makes the technique special and attractive [48, 53, 52].

As with any other combustion reaction, combustion synthesis requires the presence of an oxidizer (oxygen or any other electronegative element) and a fuel (source of reducing elements to the reaction). Because of its "redox" characteristic, combustion synthesis can be carried out via two different approaches based on the use of either redox compounds or redox mixtures [48].

The redox compounds approach uses fuel-metal complexes, which after ignition undergo self-sustained combustion to yield the desired metal oxide. The main requirement for this reaction is the presence of both the oxidizing and reducing groups together in the same compound. The combustion of ammonium dichromate ($(NH_4)_2Cr_2O_7$) is an example of this type of synthesis. This solid redox compound contains oxidizing ($Cr_2O_7^{2-}$) and reducing (NH_4^+) groups. Then, after ignition, a self-propagating and self-sustained

reaction produces the metal oxide (Cr_2O_3) in a glowing reaction known as artificial volcano:

$$(NH_4)_2Cr_2O_{7(S)} \rightarrow Cr_2O_{3(S)} + N_{2(g)} + 4H_2O_{(g)} \tag{1.10}$$

Similar to this dichromate reaction, metal complexes containing hydrazine, carboxylate, formate and acetate ions, are found to undergo self-sustained combustion. Although attractive, this method has a series of disadvantages such as preparation time (requires several days), low yield ($\approx 20\%$) and because not all metals form complexes with the hydrazine carboxylate ligand it is not possible to use this method to prepare some metal oxides (i.e., chromites, alumina) [54].

A different approach that avoids the preparation of complex mixtures makes use of the combustion of redox mixtures [54, 55]. This approach uses metal nitrates for the source of oxidizing elements and one or more energetic fuels like urea, glycine or hydrazides [48]. As an example, the so called gunpowder reaction can be used for better understanding of this exothermic and self-propagating reaction. This mixture of charcoal (fuel), sulfur (catalyst, sensitizer) and saltpeter or potassium nitrate (KNO_3) (oxidizer), discovered in China in the IX century, and part of the modern human history, can be explained in a simple equation:

$$10KNO_{3(S)} + 3S_{(S)} + 8C_{(S)} \rightarrow 2K_2CO_{3(S)} + 3K_2SO_{4(S)} + 6CO_{2(g)} + 5N_{2(g)} \tag{1.11}$$

The large amount of gases is the desired product of the reaction and act as the propellant power for a projectile.

The ratio of the oxidizer and fuel for the redox mixture is calculated using the equivalence ratio (Φ_e), defined as [56]:

$$\phi_e = O/F \tag{1.12}$$

where (O) is the total oxidizing valence and (F) the total reducing valence of the elements present in the mixture [56]. The maximum release of energy from a given mixture is reached when the ϕ_e value is equal to unity, and values higher or lower are referred as fuel rich or fuel lean mixture respectively [56]. According to propellant theory, the species M^{2+}, M^{3+}, M^{4+}, C and H are considered to be reducing with valencies of + 2, + 3,+ 4, + 4 and + 1 respectively. Oxygen is considered to be an oxidizing species with valence -2 and nitrogen is considered to be valence neutral with a value of zero [55, 56].

1.6.1 Combustion Synthesis and TiO_2

Both the above approaches for combustion, i.e., combustion of redox compounds and combustion of redox mixtures, have been used for the synthesis of TiO_2. For the first approach, titanyl hydrazine carboxylate or titanyl oxalate were used [57, 55]. The main disadvantage comes from the preparation of these complexes, which demands time and have low yield [55].

The alternative method, i.e., combustion of redox mixtures, makes use of titanyl nitrate ($TiO(NO_3)_2$) and different fuels, with ignition by gradual heating of the redox mixture in aqueous phase. Literature references for the synthesis of TiO_2 using this method together with the fuels used are listed in Table 1.1. Since the method is carried out in solution, it keeps all the advantages of the wet chemistry approach plus the capability of doping with different metal ions. Such capability has been proven in the literature for metal oxides and inorganic materials [33, 48, 58]. However, very few studies have appeared on the synthesis and doping of TiO_2 using the combustion synthesis method [53, 59, 60]. Doping was proved for carbon [53], but the use of transition metals (Cu, Fe, V, W, Zr, Ce) in form of nitrates did not achieve improvements in the photocatalytic activity of the final product [59, 60]. The use of Pt, Cu and Pd was reported to improve the photocatalytic oxidation of CO and reduction of NO [59]. Photocatalytic

Table 1.1. References and materials for synthesis of TiO_2 under combustion of redox mixtures

Oxidizing Agent	Fuel	Reference
$TiO(NO_3)_{2(aq)}$	Glycine Hexamethylenetetramine Oxalyldihydrazide	[53]
$TiO(NO_3)_{2(aq)}$	Glycine	[63, 49]
$TiO(C_2O_4).2H_2O_{(s)}$	Ammonium Nitrate	[57]
$TiO(NO_3)_{2(aq)}$	Carbohydrazide	[57]
$TiO(NO_3)_{2(aq)}$	Oxalyldihydrazide	[57]
$TiO(NO_3)_{2(aq)}$	Urea	[64]

applications of combustion synthesized TiO_2 include: degradation of poly(ethylene oxide), polyacrylamine [61], poly(bisphenol-A-carbonate) [62], and organic dyes under UV [63] or visible light [60].

1.6.2 Heterogeneous Photocatalytic Reduction of $Cr(VI)$

Because of the potential health risk from water contaminated with hexavalent chromium, local and federal regulations have been placed to increase public awareness and expand the standards for control of this pollutant nationwide. Today, almost every city has its own regulations for levels of $Cr(VI)$ in drinking water, and analyses are made on a daily basis [65]. Sources for contamination with this form of chromium are found in different industrial activities such as leather tanneries, ferrochrome production and treatment of cooling tower water.

Hexavalent ($Cr(VI)$) and trivalent ($Cr(III)$) represent the two primary oxidation states found in the environment. $Cr(VI)$ presents a high carcinogenic risk, high solubility, and high mobility, while the trivalent form has relatively low toxicity, mobility and solubility. Use of physical or chemical remediation methods like adsorption, ion exchange or precipitation does not help in the efficient removal of the toxic hexavalent chromium

from water. Instead, treatment and remediation is based on reduction to the less soluble $Cr(III)$. The most popular of these methods makes use of a strong reducing agent followed by the base precipitation as hydroxide. Other methods use direct current [66], $Fe(II)/Fe(III)$ reaction [67], or photocatalysis using titania [68, 69]. The photocatalytic method is possible because transformation from $Cr(VI)$ to $Cr(III)$ can be driven as a photoassisted reduction under UV (or visible) illumination in aqueous suspensions using TiO_2 [68].

At low pH, $Cr(VI)$ exists in aqueous solution as the dichromate anion ($Cr_2O_7^{2-}$) which can be transformed to $Cr(III)$ as shown in the equation:

$$Cr_2O_7^{2-} + 14H^+ + 6e^- \rightarrow 2Cr^{3+} + 7H_2O \tag{1.13}$$

The reduction is possible because the standard potential for ($Cr_2O_7^{2-}$) /Cr^{3+} is 1.232 V Vs. SHE [68, 70], and this value is more positive than the potential of the conduction band edge of the titania semiconductor surface. The photogenerated holes oxidize water molecules to O_2 while the electrons reduce $Cr(VI)$ to $Cr(III)$ [69]. Figure 1.7 shows a summary of events for this reacion starting from the photoexitation process.

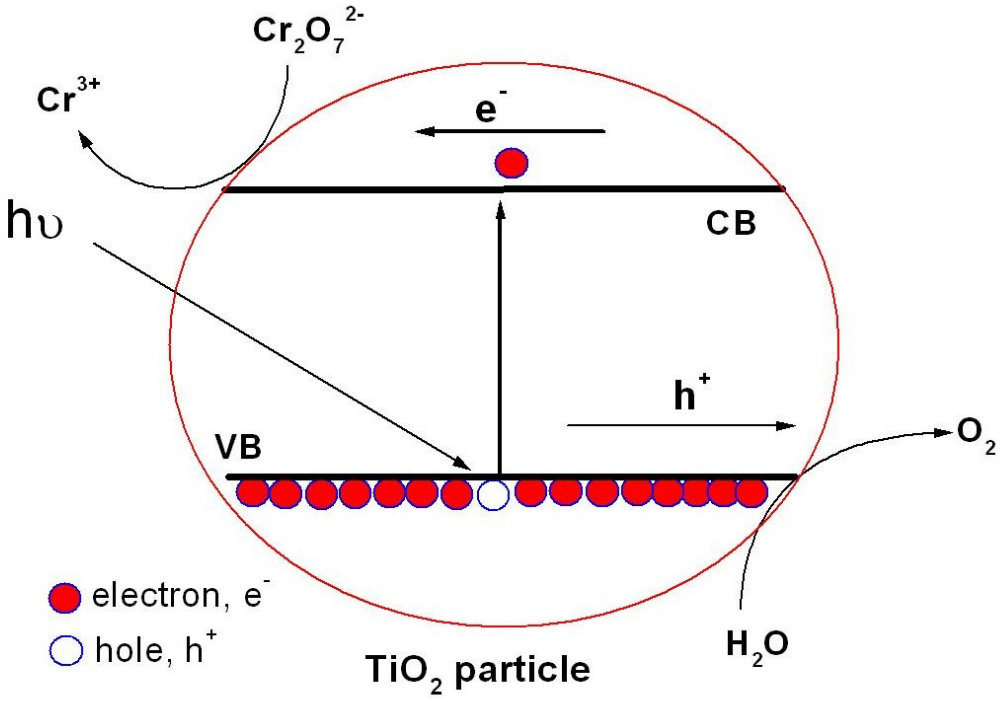

Figure 1.7. Photocatalytic reduction process of $Cr(VI)$ on a TiO_2 particle.

CHAPTER 2

EXPERIMENTAL

2.1 Chemicals

The following chemicals were used without further purification in the combustion synthesis process: Titanium (IV) oxide sulfate sulfuric acid hydrate, $TiOSO_4.2H_2O + H_2SO_4$ (Alfa Aesar 98.0 - 102.0%), urea (Sigma,ACS reagent, 99.0-100.5%), thiourea (Sigma, reagent plus 99.0%), molybdenum (V) chloride (Alfa Aesar 99.0%), titanium Sulfide, anhydrous powder (Aldrich) and TiO_2 (Degussa P-25) was used as reference in the characterization studies. The benchmark TiO_2 (Degussa P-25) was predominantly anatase and had a specific surface area of 60 m^2/g. All solutions in this study were prepared from double-distilled (Corning Megapure) water. In some instances, the samples were subject to thermal anneal at $450\,^oC$ for 30 min in air using a model 650-14 Isotemp programmable muffle furnace (Fisher Scientific).

2.2 Experimental Procedures

The synthesis of TiO_2 using combustion synthesis ($CS - TiO_2$) followed the path for the combustion of redox mixtures (see section 1.6). Urea or thiourea were used as fuels (reducing agents) and titanium oxysulfate ($TiOSO_4$) or titanyl nitrate ($TiO(NO_3)_2$) as the source for the oxidizing elements. Two sets of reactions were used with the purpose of later comparison. The first one makes use of the titanyl nitrate salt and the second one uses the oxysulfate salt. Titanyl nitrate was prepared using controlled hydrolysis of titanium isopropoxide under ice-cold water and vigorous stirring. The white precipitate ($TiO(OH)_2$) obtained was washed several times in distilled water and then dissolved in nitric acid to get a clear, transparent titanyl nitrate salt [53, 62]. In all the cases

Table 2.1. Reactants used and total oxidant/reducing ratio

Reactant	Formula	Oxidant/Reductant ratio
Titanium oxysulfate	$TiOSO_4$	-8
Titanyl nitrate	$TiO(NO_3)_2$	-10
Urea	$CO(NH_2)_2$	+ 6
Thiourea	$CS(NH_2)_2$	+ 6

stoichiometric compositions of the combustion mixtures were calculated based on the total oxidizing and reducing valencies, so that the equivalence ratio $\phi_e = O/F$ was unity [56]. Table 2.1 shows the different reagents used with the total oxidizing or reducing power of each of them. Notice that negative values represent compounds with oxidizing power while the positive ones are related to fuels with reducing power.

The reaction was started with the stoichiometric mixture of fuel and the oxysulfate or nitrate salts in a platinum crucible (water was added in the case of the oxysulfate salt). Next, the mixture in the platinum crucible was placed on a preheated hot plate (150^oC), with the objective of ensuring homogeneous mixing and starting dehydration of the aqueous mixture. Once the reaction acquired a viscous appearance, it was transferred to a preheated furnace (350^oC), where the reaction was accompanied by release of a large amount of gases producing a dry foamy, white to yellow product (See Figure 2.1).

2.3 Photocatalytic Reduction of $Cr(VI)$

For testing the photocatalytic activity, reduction of hexavalent chromium was used as a probe. The dose of photocatalyst suspension was 2 g/L in all cases. Samples were used as prepared unless otherwise expressed. An initial sparging with nitrogen for a period of 30 minutes without radiation was performed. Then the light was turned on, and the reaction was kept under constant agitation using magnetic stirring. The photoreactor used was described elsewhere [69]. The reaction vessel had an inner and

Figure 2.1. Flowchart for the combustion synthesis of TiO_2.

outer compartment. The inner quartz compartment was equipped with a water-cooling jacket that serves the purpose of housing the lamp and keeping the temperature of the vessel approximately constant. The outer compartment was an immersion well vessel with a volume of 250 mL. Nitrogen was supplied through the gas inlet to ensure efficient mixing of the suspensions.

In all instances, the total initial concentration of $Cr(VI)$ was approximately 800 μM. Samples were collected for measuring the initial concentration, and after the initial period of 30 minutes of dark equilibration. This was done with the purpose of finding the amount of chromium ion adsorbed on the surface of the catalyst. After the photoreaction was started, samples were syringed out every hour and filtered immediately after collection to remove the suspended photocatalyst (0.45 μM polytetrafluoroethylene (PTFE) syringe filter was used in each case). The solutions were analyzed using UV-vis spectrophotometry to measure the concentration of the remaining $Cr(VI)$ in the solution [68, 71].

2.4 Instrumentation

Films for XPS analysis were made using a suspension of the $CS - TiO_2$ samples and isopropanol (2-propanol containing 10 g/L dose). They were cast on the surface of indium oxide glass (ITO) by dip-coating, keeping the back surface masked with cellophane tape. After each dip, heating was performed for 10 min at 80^oC. This sequence was repeated eight times, after which the final coated films were heated overnight at a temperature of 80^oC. The $CS-TiO_2$ samples were characterized by X-ray photoelectron spectroscopy (XPS) using a Perkin Elmer/Physical Electronics Model 5000C. Scanning electron microscopy (SEM) analyses were obtained using a Zeiss Supra 55 instrument, with nominal electron beam voltage of 5 kV.

Diffuse reflectance spectroscopy was performed on a Perkin-Elmer Lambda 35 UV-vis spectrophotometer equipped with an integrating sphere. X-ray powder diffraction (XRD) patterns of the samples were obtained on a Siemens D-500 powder diffractometer using $CuK\alpha$ radiation. The step size and scan step time were set to 0.01 degree and 0.5 second respectively. Shifts of the d-spacing for the (101) peak were analyzed over a 2θ range of 22-28^o.

The source of light for the photocatalytic experiment was a tungsten halogen lamp 750 W, 120V (Sylvania) and the total Cr(VI) remaining in solution was recorded on a Hewlett-Packard Model HP 8452-diode array spectrometer.

CHAPTER 3

RESULTS AND DISCUSSION

3.1 Initial Observations

Combustion synthesis using both titanium salts (($TiO(NO_3)_2$) and ($TiOSO_4$)), were performed with urea and thiourea as fuels in the redox mixture. Two series were completed for further comparison: The first one made use of titanyl nitrate salt ($TiO(NO_3)_2$) plus urea (NU), thiourea (NT), or mixtures of both fuels (NUT). For the second series, stoichiometric mixtures of the oxysulfate salt ($TiOSO_4$) plus urea (SU), thiourea (ST), or mixture of fuels (SUT) were used. In both cases, the final product was a white to yellow solid with foamy appearance (see Figure 3.1).

Comparison of oxidizing materials (($TiO(NO_3)_2$) and ($TiOSO_4$)) in the various reactions shows no apparent difference other than reaction time. On the other hand, a strong influence was found when the two different fuels were compared, giving in all instances a bright yellow, dense and compact solid material when thiourea was used in the reaction. In contrast, the use of urea results in a more foamy voluminous solid material with white to pale yellow color. All reactions proceeded in the same fashion; on heating, the precursor mixture turned from cloudy to clear, then initial evaporation of the solvent was observed. The samples were then transferred to the furnace, where the reaction between the fuel and titanium salt proceeded with the generation of heat, flame and gases. The final appearance of the $CS - TiO_2$ samples prepared in the oxysulfate series can be seen in Figure 3.1, where the upper part is the benchmark TiO_2 Degussa P-25 sample, the white powder in the left side is from reaction with urea (SU), the

Figure 3.1. Physical appearance of $CS - TiO_2$ for the oxysulfate series. See text for identification.

sample in the right side is from reaction with thiourea as fuel (ST), and the picture in the bottom is of the final powder using a mixture of the two fuels (SUT).

Titanyl sulfate and nitrate salts were also dissolved in a precursor solution without any fuel, in order to find out if any reaction occurs in absence of the reducing elements. Procedure was as described above, but no reaction was observed. In addition, even though some material remained on the walls of the crucible after heating inside the furnace, no combustion reaction was detected during this time.

3.2 Combustion Synthesis of TiO_2

The first set of reactions were made using $TiO(NO_3)_2$ with urea, thiourea as fuel, or a mixture of these two fuels. The second set of reactions involved $TiOSO_4$ as the source for oxidizing elements and same fuels mentioned above. Characterization of the products of the different reactions and its photocatalytic activity will be addressed in the following subsections.

3.2.1 Diffuse Reflectance Spectroscopy

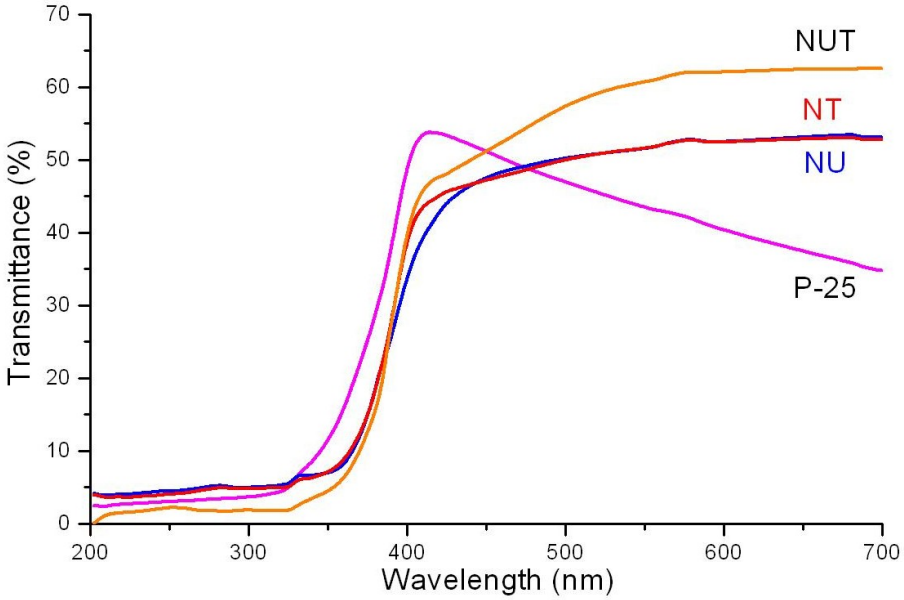

Figure 3.2. UV-visible diffuse reflectance spectra for the various $CS - TiO_2$ samples using $TiO(NO_3)_2$ and different fuels.

Figure 3.2 and 3.3 contain the UV-visible transmittance spectra recorded for films formed from the $CS - TiO_2$ samples prepared using different precursors and fuels. A dramatic change can be observed for the $TiOSO_4$ series (Figure 3.3). Specifically, a

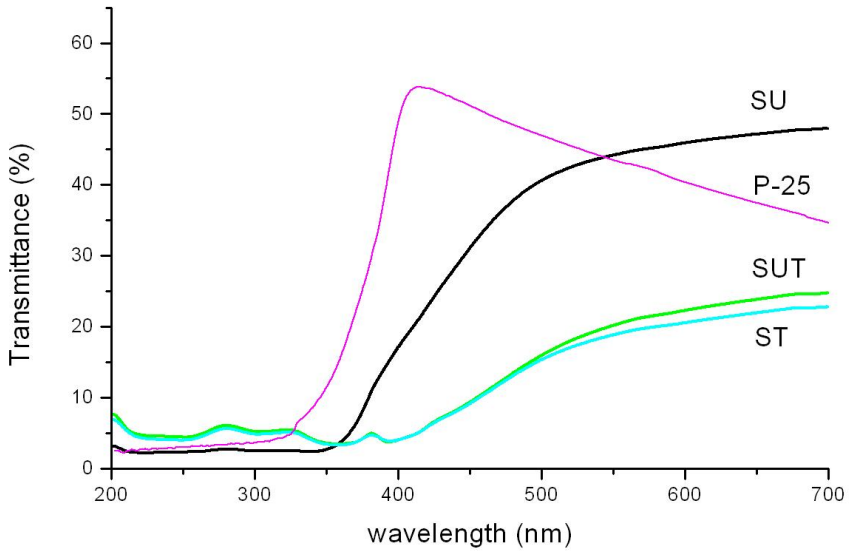

Figure 3.3. UV-visible diffuse reflectance spectra for the various $CS - TiO_2$ samples using $TiO(NO_3)_2$ and different fuels.

decrease in transmittance is found in 380 - 700 nm range for samples prepared from the oxysulfate salt when compared with the benchmark TiO_2 (Degussa P-25). On the other hand, the series prepared from the titanyl nitrate salt showed a more modest improvement in the absorption of light (see Figure 3.2). In general both series present improvement in the absorption of visible light by TiO_2 with a shift to the red spectral region.

To determine the band gap of each sample, the variation of $(\alpha h\nu)^2$ with excitation energy $(h\nu)$ was obtained using the diffuse reflectance data for the various films. Intercepts of the Tauc plots [72] show the approximate values of the optical band gap (E_g) for the two different series. These plots are shown in Figure 3.4 and 3.5, where TiO_2 P-25 serves as the reference with a band gap value (3.3 eV) in agreement with values reported elsewere [3, 4].

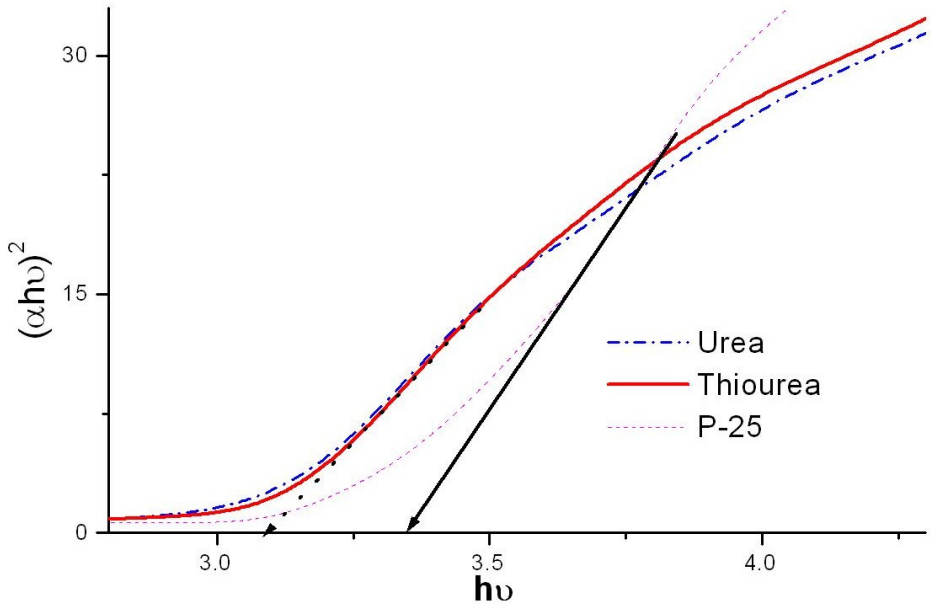

Figure 3.4. Tauc plots for the $TiO(NO_3)_2$ series.

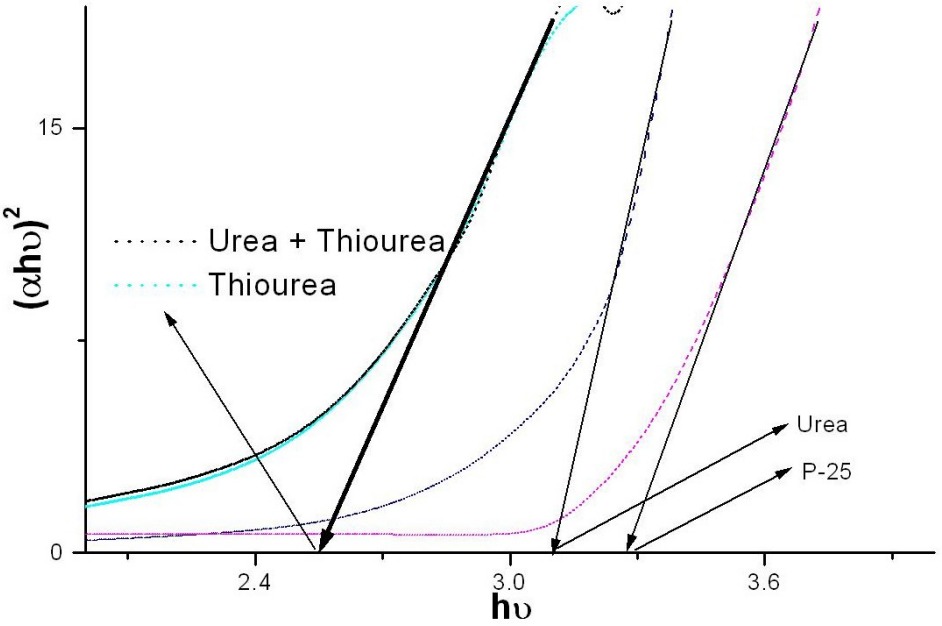

Figure 3.5. Tauc plots for the $TiOSO_4$ series.

Table 3.1. Band gap values obtained for the various $CS - TiO_2$ samples. See text for sample notation

Sample	$E_g(eV)$
P-25	3.3
SU	3.1
ST	2.5
SUT	2.5
NU	3.1
NT	3.1
NUT	3.1

It is rather remarkable that using urea or thiourea as fuel did not make any difference in the band gap of $CS - TiO_2$ for the titanyl nitrate series ($\approx 3.1\, eV$). In fact, no change is seen in the Tauc plots for the two cases (Figure 3.4). In the case of $TiOSO_4$ a value of 3.1 eV was obtained for urea (SU), while with the use of thiourea (ST) or a mixture of fuels (SUT), the value of the band gap was reduced to 2.5 eV (see Figure 3.5).

The band gap values (E_g) for the various $CS - TiO_2$ samples are compared in Table 3.1 along with the value for the reference TiO_2 (Degussa P-25) sample. A general improvement is observed in the absorption of light in the visible region for all the samples. The change in band gap is appreciable for the samples from the combustion reaction of titanium oxysulfate salt with thiourea or a mixture of urea and thiourea.

3.2.2 XPS

X-ray photoelectron spectroscopy (XPS) was used to study the chemical states of the different elements and the nature of doping of the $CS - TiO_2$ samples. XPS is a well established non destructive surface analysis technique for crystalline and amorphous materials. It permits the determination of the oxidation states of elements in a sample.

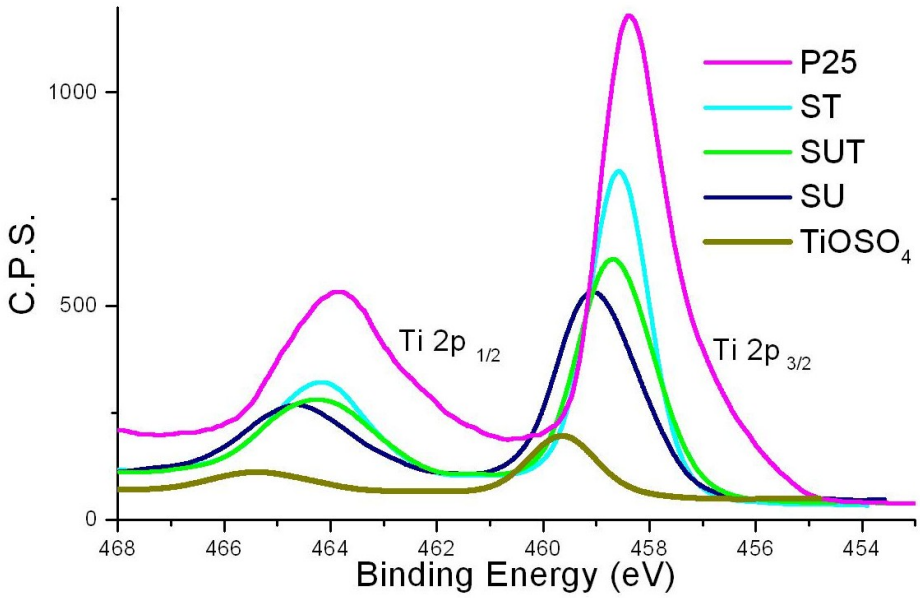

Figure 3.6. High resolution XPS of $Ti\ 2p$ core level for $CS - TiO_2$ and Degussa P-25 sample.

To understand the different oxidation states, a set of reference materials and different products were prepared using the dip coating technique [73]. The reference materials included titanium oxysulfate ($TiOSO_4$), titanium disulfide (TiS_2) and a physical mixture of Degussa P-25 TiO_2 and 5.0 % elemental sulfur ($TiO_2 + S$)). The $CS - TiO_2$ samples were made using the two different precursor salts and various fuels as discussed earlier.

Calibration spectra for all the samples was made using the $C\ 1s$ line at 284.6 eV, which was present as a strong signal and is assigned to adventitious surface carbon [74]. Accompanying this peak, the $C\,1s$ spectra for all the samples (references and $CS-TiO_2$) show two extra peaks at 285.5 and 288.5 eV. These peaks could be assigned to elemental carbon in the case of the first signal and carbonate species to the peak around 288 eV. Importantly, no peak around 282 eV is present indicating the absence of $Ti - C$ bond and precluding doping by carbon in the samples [53, 75].

The $N\,1s$ peak was also recorded for all $CS-TiO_2$ samples, the peak with low intensity and position around 400 - 401 eV is assigned as an amino group present in the final product and is in agreement with values in the literature [53, 74, 76]. No peak at 396 eV was found showing the absence of nitrogen doping in the final product [14].

The $Ti\,2p$ level spectra for all samples show the typical two peaks for $Ti^{4+}(2p_{\,3/2})$ and $Ti^{4+}(2p_{\,1/2})$. Furthermore, all samples showed the typical energy difference between the two peaks ($\Delta Eb = Eb(Ti2p_{\,1/2}) - Eb(Ti2p_{\,3/2})$) with a value around 5.7 eV [74]. Also, the intensity ratio between them is close to the 1:2 value reported for spin-orbital splitting [30, 74]. These peaks are listed in Table 3.2 and the spectra are presented in Figure 3.6.

The reference TiS_2 sample, representing a titanium in a sulfur rich environment shows two peaks for Ti^{4+} at lower binding energy (455.8 - 462 eV) plus an extra peak corresponding to contamination from the oxide form of titanium ($Ti-O$ bond) which is mainly due to the preparation method of the film [77]. The oxygen rich environment represented by the reference TiO_2 (Degussa P-25) appears at a higher energy with peaks centered at 458.4 and 463.8 eV plus a peak related to Ti^{3+} around 457 eV [78]. The Ti peak for $TiOSO_4$ appears at 459.4 and 465.4 eV reflecting the rich oxygen and sulfur environment surrounding the metal ion ($Ti-O-S$ and $Ti-O-Ti$ bonding) in agreement with its structure [79].

From Table 3.2 a change in position for the $Ti\,2p_{\,3/2}$ signal can be observed for the different samples prepared via combustion synthesis. Specifically the NU, ST and SUT samples show a shift from the value associated with the peak for $TiOSO_4$ (459.6 eV) to a value close to the reference TiO_2 (458.2 eV) case.

The $O\,1s$ region spectra for $CS-TiO_2$ shows a broad shape that reveals a complex composition for the different samples and references. This complexity can be resolved for each peak by means of curve fitting, the resulting distribution is a convolution of

Table 3.2. XPS analysis details for the $Ti\,2p$ peak for reference and $CS-TiO_2$ samples

Sample	Binding Energy (eV)	Peak Designation	Area	ΔEb	FWHM
TiS_2	458.3	$Ti-O$	173	5.7	1.2
	464		152		2.3
	455.8	$Ti-S$	411	6	1.1
	461.9		225		1.6
TiO_2	458.2	$Ti-O$	1908	5.6	1.8
	463.8		865		2.2
	456.8	Ti^{3+}	188		1.1
$TiOSO_4$	459.6	$Ti-O-S$	222	5.7	1.2
	465.3		98		2.0
NU	458.4	$Ti-O$	1041	5.6	2.0
	464.0		478		2.5
NT	459.3	$Ti-O$	239.2	5.7	1.6
	465.0		126		2.6
SU	458.9	$Ti-O$	885	5.6	1.7
	464.5		420		2.4
ST	458.5	$Ti-O$	1619	5.7	1.1
	464.2		505		2.0
SUT	458.6	$Ti-O$	952	5.6	1.5
	464.2		472		2.3

the individual contributions to the overall peak [74]. For example, the reference (TiO_2) P-25 has two main peaks contributing to the core level, which are in accordance with values reported in the literature [53, 74] and can be assigned as the binding energies for oxygen-metal bonding (around 529.5 eV) and to the presence of hydroxyl groups (OH^-) adsorbed on the TiO_2 surface (532.4 eV) [53, 76].

Deconvolution for $TiOSO_4$ reflects the inner composition of the oxysulfate with a ternary constitution as seen in Figure 3.7. Here, I represents the binding energy for the oxide (at 530.5 eV), II represents the OH^- signal around 531.7 eV and III is the $S-O$ region that corresponds to sulfate and bisulfate groups with a value of 532.6 eV [74, 80]. These values are consistent with the structure of the titanium oxysulfate salt [79].

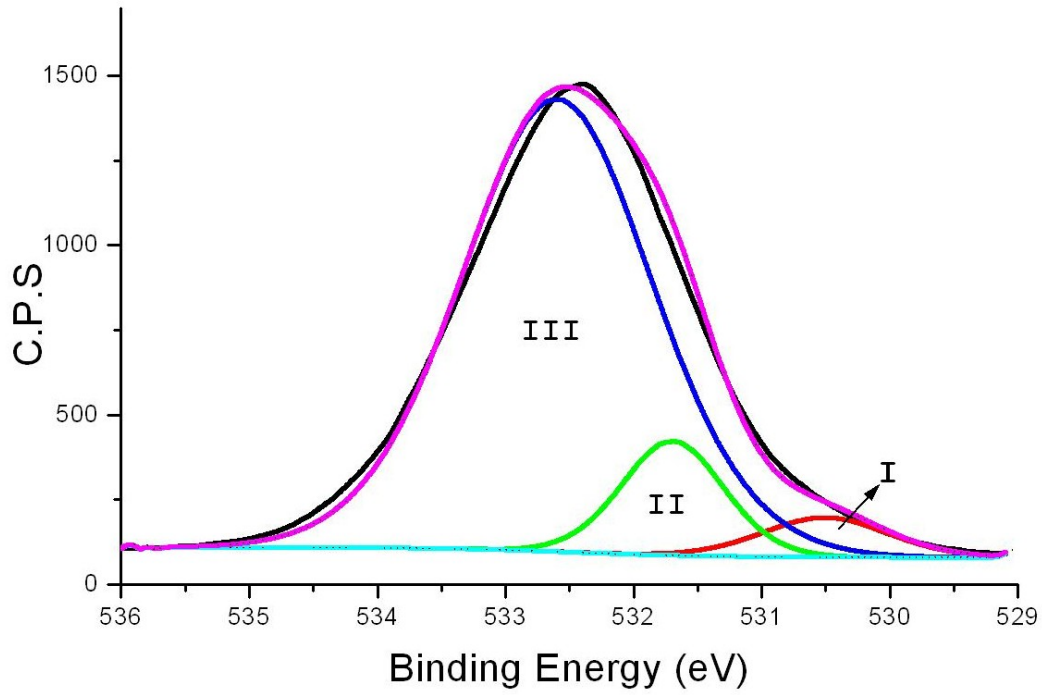

Figure 3.7. Deconvolution of the O 1s core level spectrum for $TiOSO_4$ reflecting its composition. The components I, II, III are elaborated in the text.

For the case of $CS - TiO_2$ the same analysis was applied and curve fitting gave a ternary composition as exemplified by the SUT sample in Figure 3.8. In this case the lower binding energy (represented by I) is again related to oxygen in the oxide while the higher binding energy (III) can be attributed to oxygen as sulphate groups. Component II is assigned to OH^- groups adsorbed on the surface and has a value of 531.4 eV. These peak deconvolution analysis show in particular a high concentration of sulfate related species and low hydroxide or oxide participation for the oxysulfate salt again in agreement with the structure of this soluble salt [79]. For the $CS - TiO_2$ samples the highest presence of $O - S$ groups is observed for the SU sample while the highest OH^- levels are observed for the SUT sample.

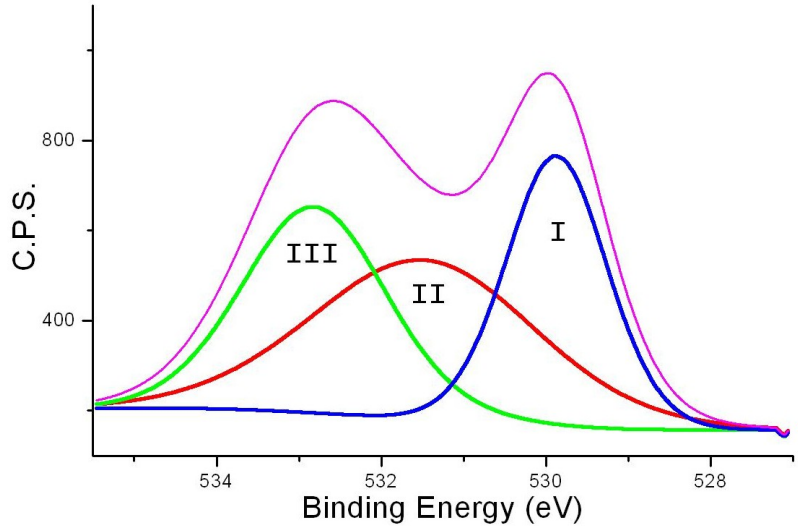

Figure 3.8. $O\ 1s$ core level spectrum deconvoluted to show the different components for the SUT sample. The components I, II, III are elaborated in the text.

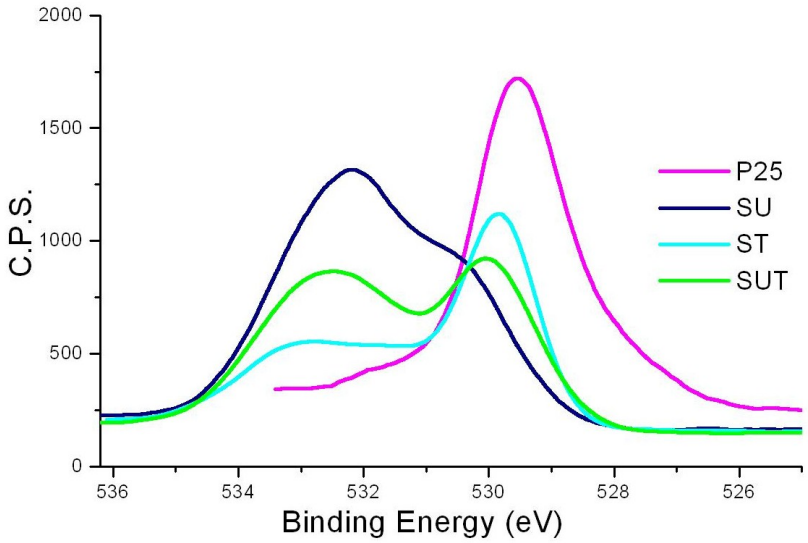

Figure 3.9. High resolution XPS of $O\ 1s$ core level for $CS - TiO_2$ and Degussa P-25 samples.

Table 3.3. Binding energy values of components in the $O1s$ spectra of different $CS-TiO_2$ and reference materials

Sample	Binding Energy (eV)	Area	Peak Designation	FWHM
TiO_2	529.5	2646	$Ti-O$	1.7
	530.8	106	OH^-	1.0
$TiOSO_4$	530.5	146	$Ti-O$	1.5
	531.7	342.5	OH^-	0.9
	532.6	2532	$S-O$	1.7
NU	529.5	920	$Ti-O$	1.6
	530.5	636	OH^-	2.4
NT	529.8	1353	$Ti-O$	1.2
	531.3	273	OH^-	1.2
	532.8	892	$S-O$	2.3
SU	530.1	944	O^{2-}	1.7
	531.5	747	OH^-	2.3
	532.5	2201	$S-O$	2.2
ST	529.8	1353	$Ti-O$	1.2
	531.3	273	OH^-	1.2
	532.8	892	$S-O$	2.3
SUT	529.9	934	$Ti-O$	1.4
	531.4	1219	OH^-	3.0
	532.8	1020	$S-O$	2.1

Figure 3.9 shows the O $1s$ core level in the oxysulfate series together with the reference TiO_2. Values for the different reference and $CS-TiO_2$ samples materials with the curve fitting analysis, peak designation and area are given in Table 3.3.

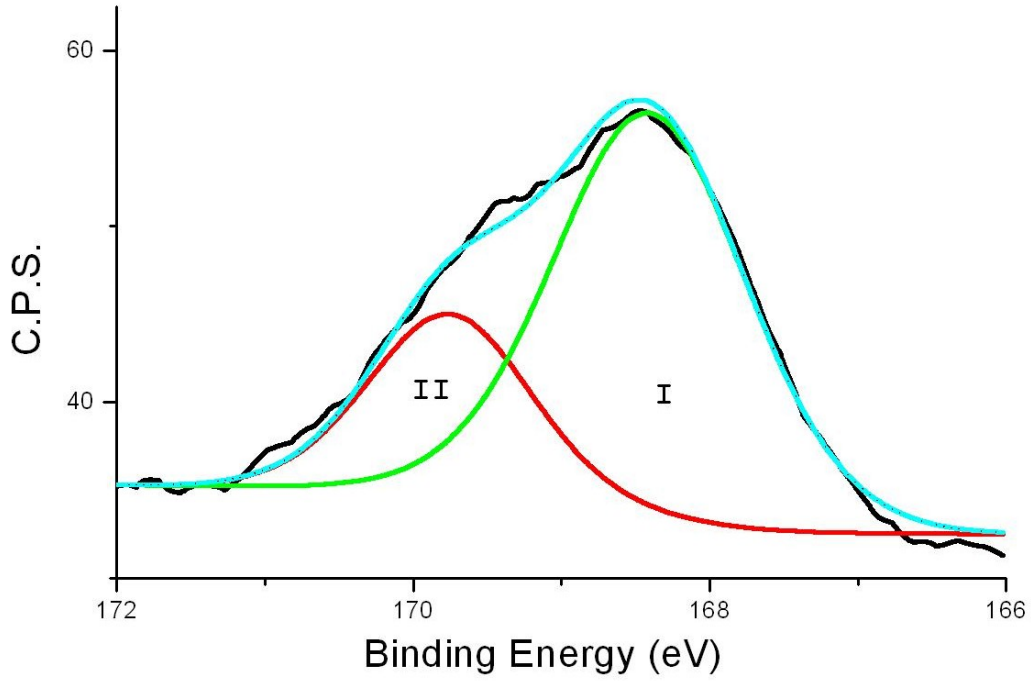

Figure 3.10. Deconvolution of the $S\ 2p$ core level spectra for the SUT sample. I and II are identified in the text.

The $S\ 2p$ core level spectra for the different samples and references were also recorded and the values are reported in Table 3.4. Once again, deconvolution of the peak reveals the complex chemical composition. Figure 3.10 is an example of this; it represents the curve fitting for the SUT sample. Area I with value around 168.6 eV is assigned to the presence of S in the 4+ state (S^{4+}) and 169.5 eV corresponds to the S^{6+} species [25, 74, 81-83]. The binding energy values for both components are in agreement with data in the literature [74, 81].

From the reference samples the values for the binding energy of sulfur in a titanium rich environment represented by TiS_2 was found to be in agreement with values reported (160 - 161 eV) [77, 81]. The physical mixture of Degussa P-25 and elemental sulfur (5.0 %) showed two broad peaks with low intensity related to the presence of sulfur; the first around 163 eV representing elemental sulfur in the sample while the peak at 168 eV

Table 3.4. S 2p Binding energies, relative percentages in for $CS - TiO_2$ samples, with curve fitting analysis. (*) Represents elemental sulfur

Sample	Position (eV)	Peak Designation	Conc.%	Area	FWHM
TiS_2	160.3	$Ti - S$	63.5	295.4	0.67
	161.5	S^{2-}		197	0.86
	162.9	S^{*}		17	1.0
$TiO_2 + S$	162.8	S^{*}	2.5	46	3.0
	168.1	S^{+4}		25	2.5
$TiOSO_4$	168.8	S^{+4}	10	38	0.9
	169.4	S^{6+}		199	2.1
NT	168.5	S^{+4}	13	96	1.3
	169.5	S^{6+}		103	1.7
SU	168.5	S^{+4}	6.7	108	1.6
	169.6	S^{6+}		115	2.0
ST	168.1	S^{+4}	1.4	22	1.5
	169.8	S^{6+}		10	1.2
SUT	168.5	S^{+4}	2.0	38	1.5
	169.8	S^{6+}		13	1.2

is related to the sulfur as the SO_2 species. These values again are in agreement with references in literature [74, 77, 81].

Figure 3.11 shows different peaks for the $CS - TiO_2$ samples in the titanium oxysulfate series along with $TiOSO_4$ as reference. Examination of the shape reveals a high content of sulfur as S^{6+} for the $TiOSO_4$ reference and the sample prepared using the oxysulfate salt and urea as fuel (SU), proving the presence of sulfate species in these two samples as S^{6+}. In fact, the area in the XPS spectra for S^{6+} is up to 5 times more than that for S^{4+} for this samples. This is in agreement with the structure of this soluble salt (see Figure 3.12) [79].

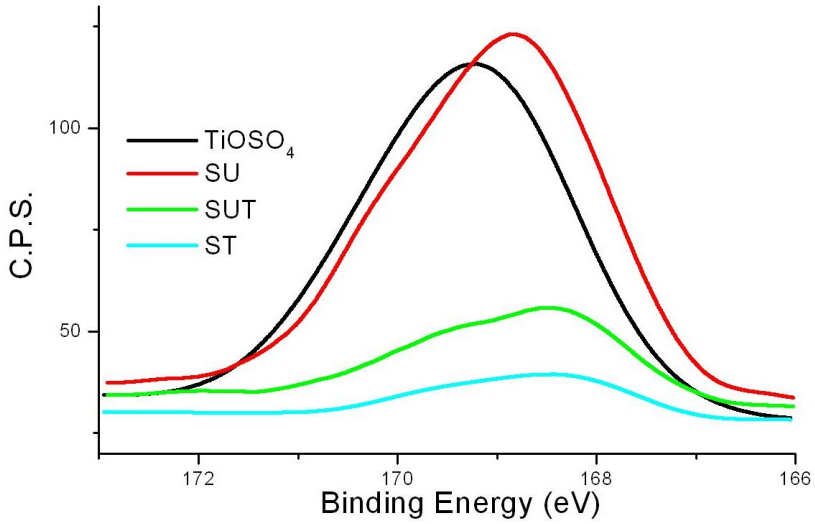

Figure 3.11. $S\ 2p$ spectra of $CS - TiO_2$ samples in the oxysulfate series.

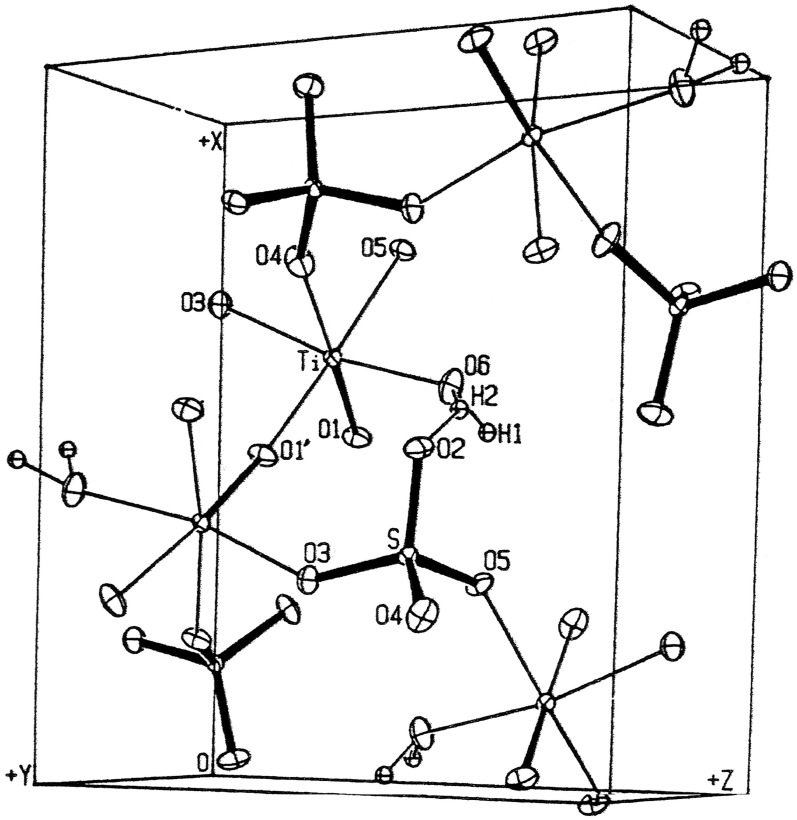

Figure 3.12. Structure of hydrated titanyl sulfate [79].

The total concentration of sulfur in the surface, binding energy positions and peak designations for the various samples are presented in Table 3.4. Using values obtained for peak area a comparison of the ratio of sulfur species (S^{4+}/S^{6+}) can be made for the various $CS-TiO_2$ samples. Thus, values close to unity can be found for NT and SU samples while ST and SUT samples present two and three times more S^{4+} species (see Table 3.4).

As a conclusion for this part of the the work, sulfur was found to be present in the different $CS-TiO_2$ samples as a mixture of oxidation states (S^{4+} and S^{6+}) with values of binding energy around 168.5 and 169.5 eV respectively in agreement with references found in literature [24-26, 82] . Importantly, S^{2-} species (binding energy around 161-162 eV) were not found in the $CS-TiO_2$ samples precluding the substitution of sulfur atoms for the oxygen atoms in titania host lattice [23]. A high fraction of sulfur occurs in the 6+ oxidation state in the $TiOSO_4$ reference salt and the sample prepared using the oxysulfate salt and urea SU. On the other hand, ST and SUT samples show a stronger presence of the 4+ oxidation state. The $CS-TiO_2$ the sample prepared with the oxysulfate salt and a mixure of the two fuels (SUT) presents the highest ratio of S^{4+} to S^{6+}.

A set of samples were prepared in the SUT series with the purpose of studying the effect of washing of the final sample. Films were prepared with the as prepared sample and after washing with DI water several times, then the XPS spectra were recorded and compared.

For the $Ti\ 2p$ core level spectrum no significant change in the binding energy occurred and a constant ΔEb value of 5.7 eV was identified for the $Ti\ 2p$ spin-orbital splitting [30, 74]. The $O\ 1s$ core level for the as prepared and after washed samples are compared in Figure 3.13. The values obtained after peak deconvolution show no change in the binding energy positions for the different curves (see Table 3.5). Furthermore,

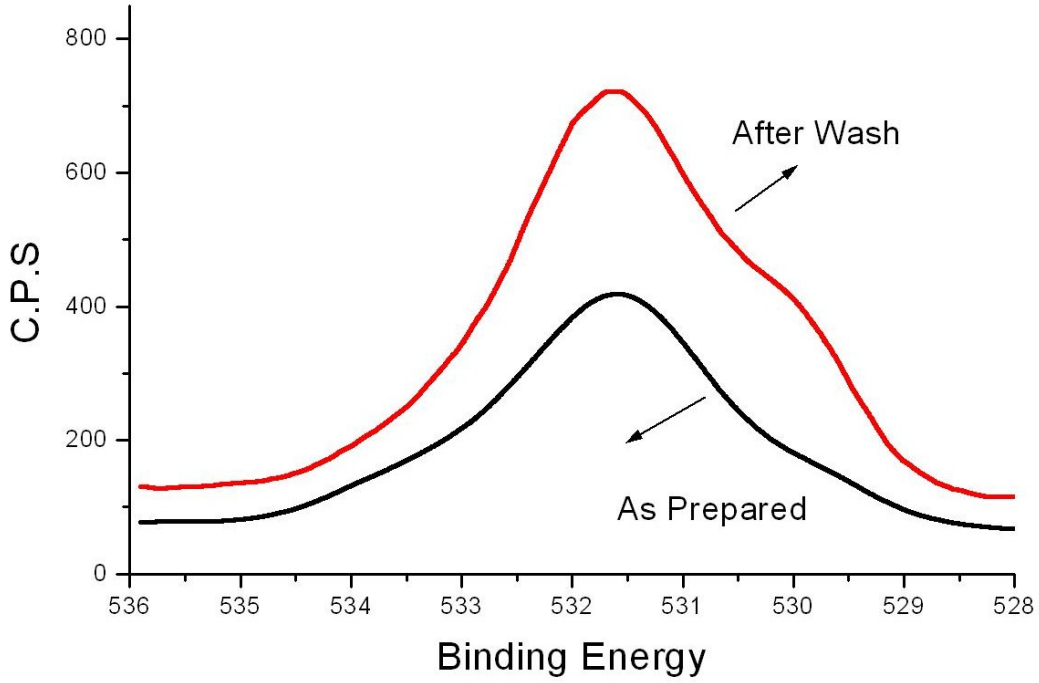

Figure 3.13. XPS $O\,1s$ core level spectra for SUT sample as prepared and after washed.

peaks related to the metal oxygen ($Ti-O$) bond and OH^- groups (529 and 531 eV respectively) on the surface increase for the washed sample. On the contrary, the value related to the presence of $O-S$ (533 eV) was reduced in the washed sample (see Table 3.5).

For the $S\,2p$ core level a reduction in the peak area at 169-170 eV was observed for the washed sample along with an increase in the area around 168 eV. This is clear indication of a reduction of the S^{6+} groups for the washed sample and an increase in the S^{4+} presence. Figure 3.14 shows the $S\,2p$ core level spectra for the two samples. The three solid curves represent the sample after the washing process (black curve), and the curves obtained from peak deconvolution showing the presence of S^{6+} (red curve) and S^{4+} (blue curve). The dashed curve represents the as prepared sample. Binding energy values and peak assignments for these curves are contained in Table 3.6. When

Table 3.5. $O\ 1s$ core level XPS data for the $CS - TiO_2$ samples showing the effect of post-synthesis washing

Sample	Binding Energy (eV)	Area	FWHM
As prepared	529.9	123	1.5
	531.5	572.5	1.6
	532.9	260	2.2
After wash	529.9	307	1.3
	531.6	1245	1.9
	533.3	127	1.7

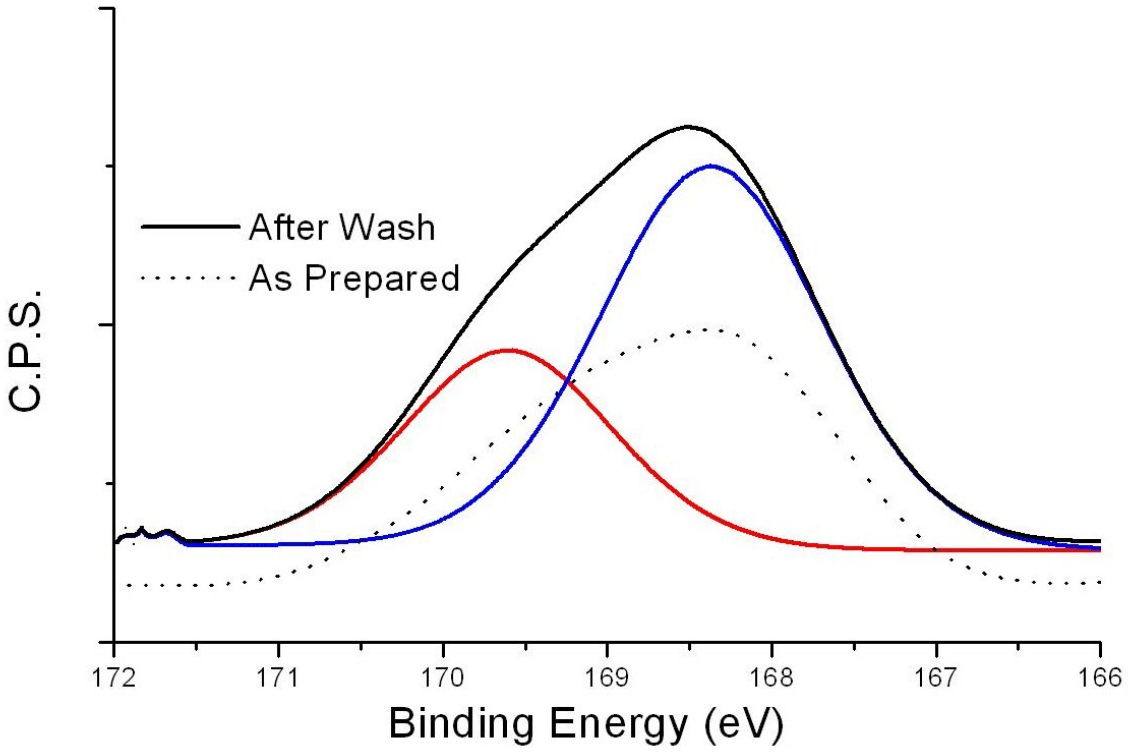

Figure 3.14. $S\ 2p$ core level spectrum of SUT sample showing the effect of washing.

Table 3.6. Binding energy (BE) for the $S\,2p$ core showing the effect of washing

Sample	Binding Energy (eV)	Area	Peak Designation
As Prepared	168.1	33.5	S^{4+}
	169.1	68.1	S^{6+}
After washed	168.4	104	S^{4+}
	169.6	50	S^{6+}

comparing the overall elemental composition for both samples, a small change in the ratio of the different elements present at the surface of the samples was observed. The ratio was calculated for $O : Ti : S$ as 10:1:2 for the as prepared sample while the post-synthesis washed sample showed values of $\approx 6 : 1 : 1$.

As a summary of the XPS study, cationic doping by means of sulfur was found in the samples prepared by combustion synthesis, the oxidation states of the S atoms incorporated into the titania structure were determined to be S^{6+} and S^{4+}. The $O\,1s$ core level data revealed abundance of OH^- groups relative to $Ti - O$. Since XPS is a surface technique this implies the presence of plentiful hydroxyl groups on the surface while the $Ti - O$ contribution arises from the catalyst bulk. Neither carbon nor nitrogen doping was noted based on values of binding energies. Substitution of sulfur for titanium in the structure of TiO_2 was also not observed. A general increase in peak area for the washed sample was found with no change in position for the oxygen or titanium core levels. Sulfur as S^{4+} species remains after washing several times with deionized water. Same trend appears for the $O\,1s$ core level of the as prepared and washed samples, with increase up to four times in area for the $O - Ti$ (529.9 eV) and OH^- (531.5 eV) signals, and a decrease in the total area for $O - S$ at 533 eV (see Figures 3.13 and 3.14).

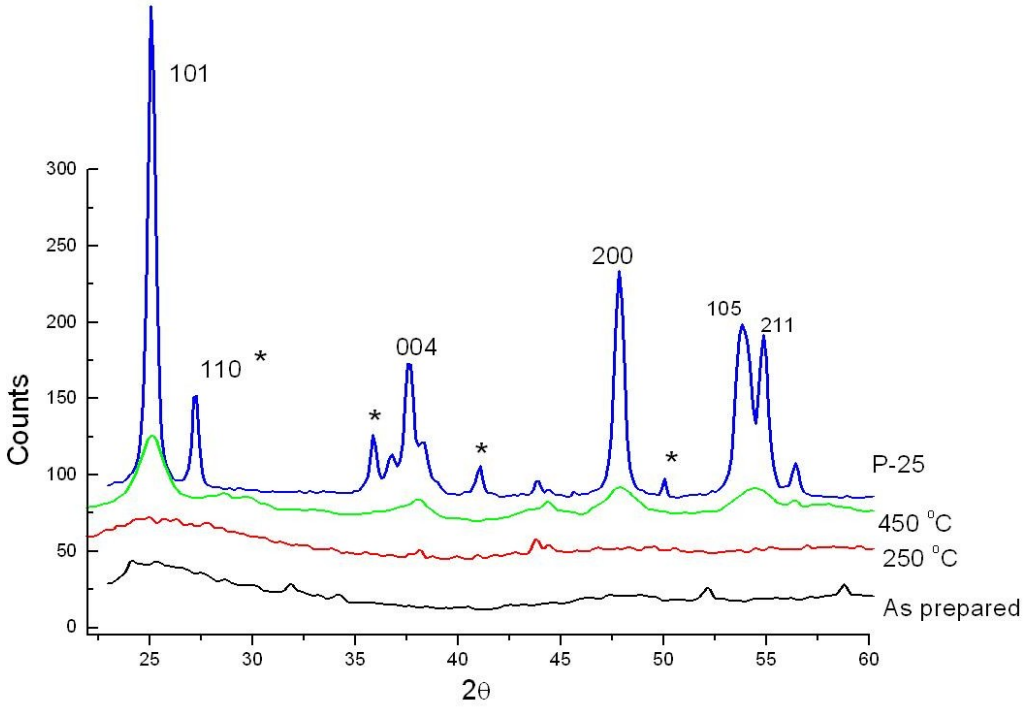

Figure 3.15. Powder XRD patterns showing the effect of annealing for the *ST* sample.

3.2.3 XRD

Figure 3.15 shows the powder X-ray diffraction patterns showing the effect of annealing for the ST sample. It can be seen that the as prepared sample shows amorphous characteristics and an increase in crystallinity is obtained after annealing at 450 ^oC. A similar trend was found for the *SUT* sample, but in the *SU* case, the initial amorphous characteristic did not change even after annealing at 450 ^oC. The position of the (101) peak reflects the trend in crystallinity as seen in Figure 3.15.

Figure 3.16 shows XRD patterns of reference TiO_2 (Degussa P-25) (predominantly anatase) along with the sample prepared using the mixture of fuels (*SUT*). For the *ST* and *SUT* samples the initial amorphous material has anatase composition after the annealing process (see Figure 3.16). Interestingly, annealing to a temperature up to 750 ^oC shows no appreciable conversion to the rutile phase in the *SUT* sample (see

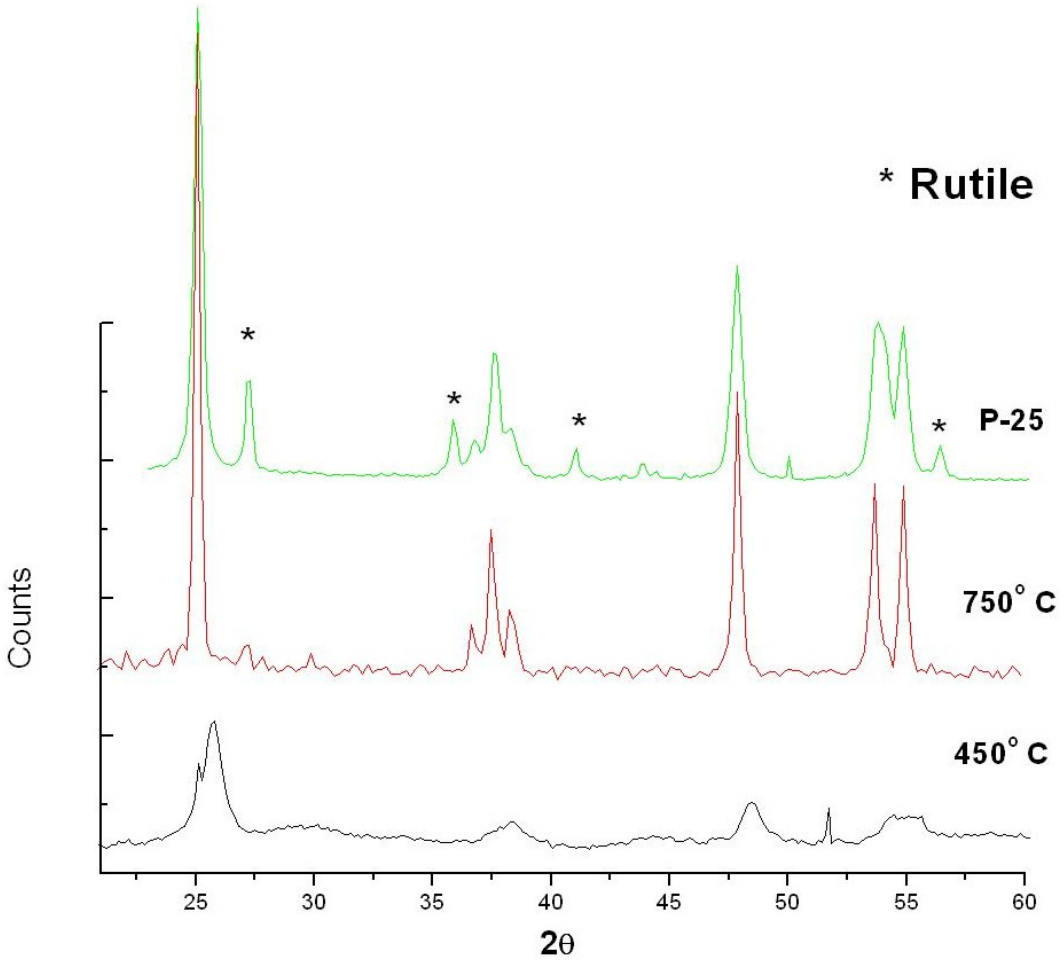

Figure 3.16. Annealing effect of the *SUT* sample. (*) Denotes peak assigned to rutile structure and all the other peaks correspond to anatase phase.

Figure 3.16). This phenomenon was pointed out in the literature for doping of TiO_2 with sulfur, concluding that presence of sulfur in the grain boundaries prevent the phase transition of anatase to rutile [84].

Values for position of the peak and crystallite sizes of the samples were calculated using the (101) signal for the *SUT* and *ST* annealed for 30 minutes at 450^oC, Degussa P-

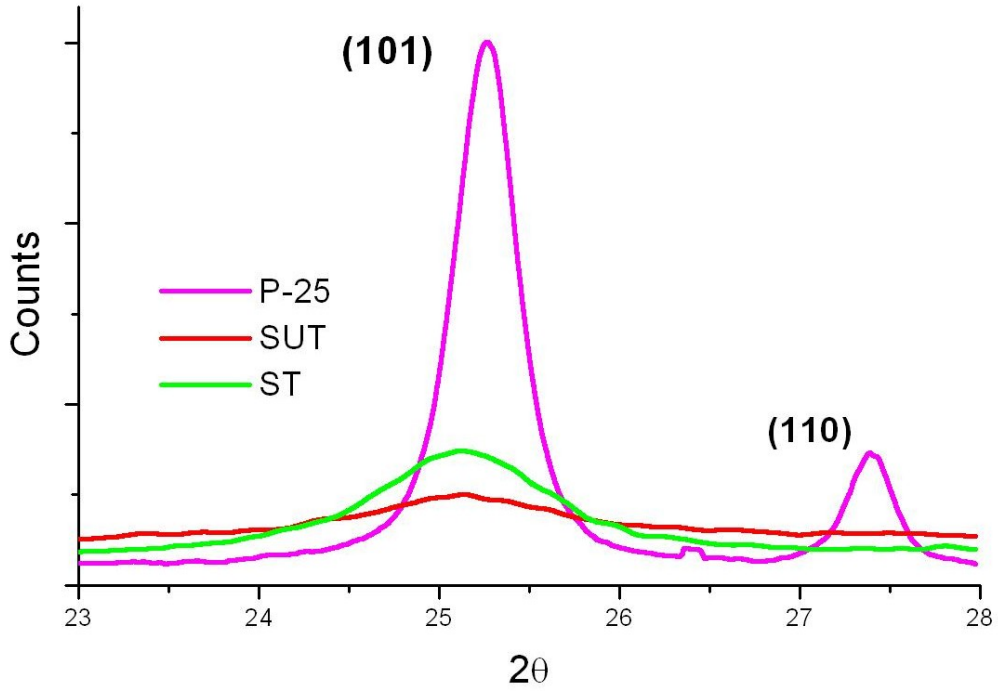

Figure 3.17. Comparison of Degussa P-25 TiO_2 with ST and SUT samples for the (101) XRD peak.

25 was used as reference. The average crystalline sizes of the two samples was estimated from the (101) peak of anatase using the Debye-Scherrer equation:

$$D = \frac{K\lambda}{\beta \cos\theta} \mathring{A} \tag{3.1}$$

where D is the average crystallite size in angstroms, K is a constant (0.89), λ is wavelength of copper $K\alpha$ (1.5405 Å), β is the full width at half maximum (in radians)($1^o = \pi/180\, radians$), and θ is the diffraction angle. The calculated values together with the position of the (101) peak and the FWHM values are shown in Table 3.7.

The particle size in Degussa P-25 was found to be 21.2 nm in size in agreement with values reported elsewhere [85]. High resolution analysis of the (101) signal of Degussa P-25 and the ST and SUT samples annealed to 450 ^oC reveal a shift in the position of

Table 3.7. Comparison of grain size for SUT and ST samples with Degussa P-25

Sample	2θ	FWHM	Grain size (nm)
P-25	25.30	0.38	21.2
ST	25.15	1.19	5.5
SUT	25.15	1.19	6.7

the (101) signal (see Figure 3.17). This could be related to lattice distortion in the doped samples. Further analyses of these peak shifts are required and this work is in progress.

3.2.4 SEM

Figures 3.18 and 3.19 contain representative SEM images for the sulfate series of samples prepared with either a mixture of the two fuels (Figure 3.18) or with urea alone (Figures 3.19). The samples prepared using thiourea (either alone or in combination with urea) present a mesoporous morphology with many pores which presumably result from the evolved gas during the combustion (see Figure 3.18, for example). On the other hand when urea is used as the fuel, no pores were observed and only a melted solid appearance is observed. This is exemplified by the micrograph in Figure 3.19. The morphology as probed by SEM for the $CS-TiO_2$ samples is markedly different from the Degussa P-25 case shown in Figure 3.20.

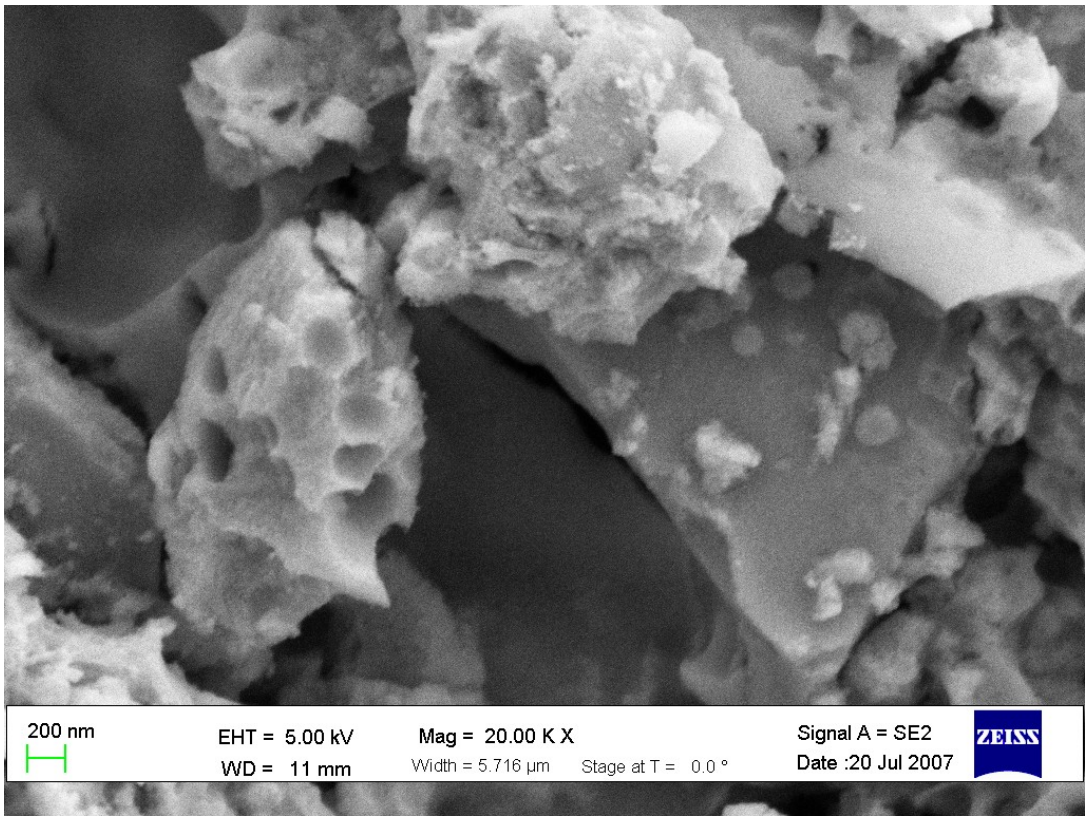

Figure 3.18. SEM image of as-prepared *SUT* sample.

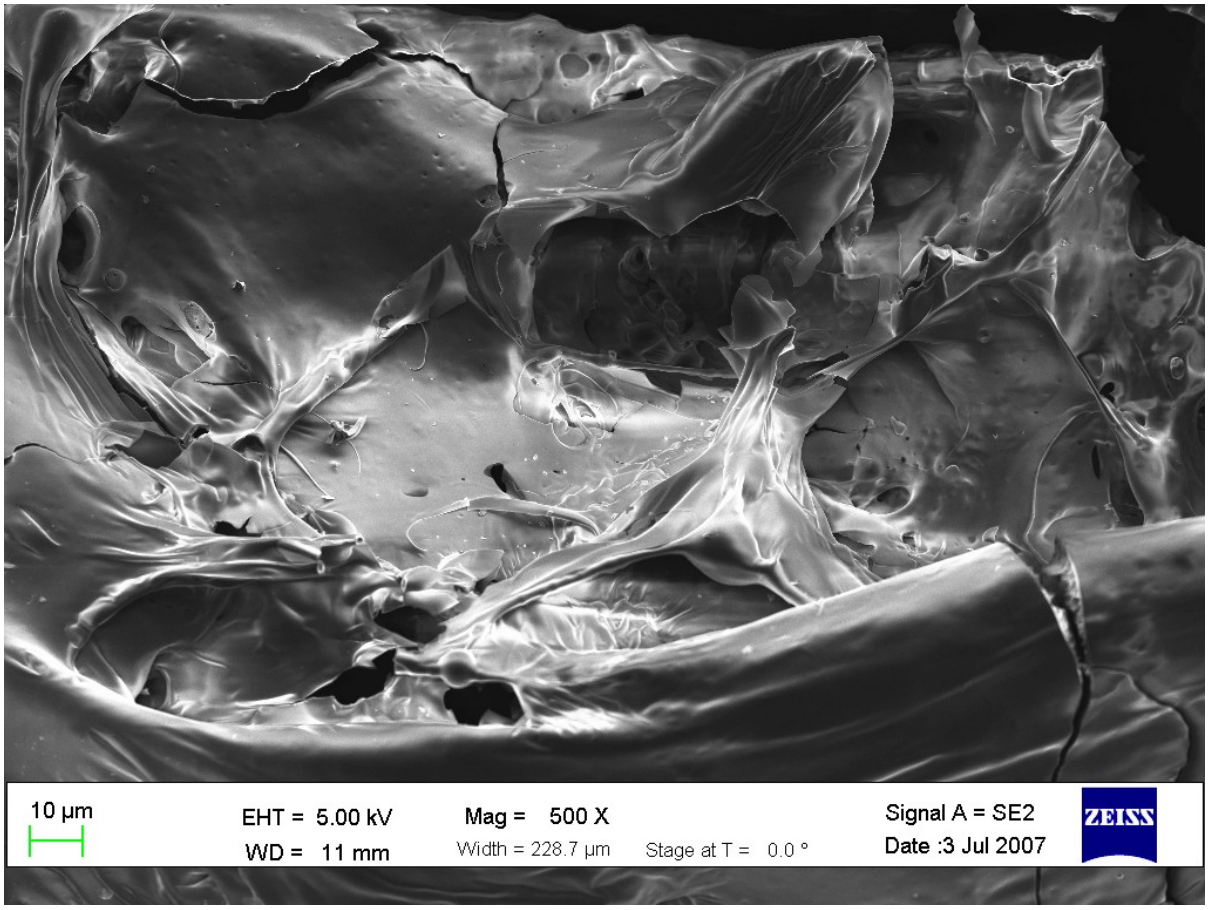

Figure 3.19. SEM image of an as-prepared *SU* sample.

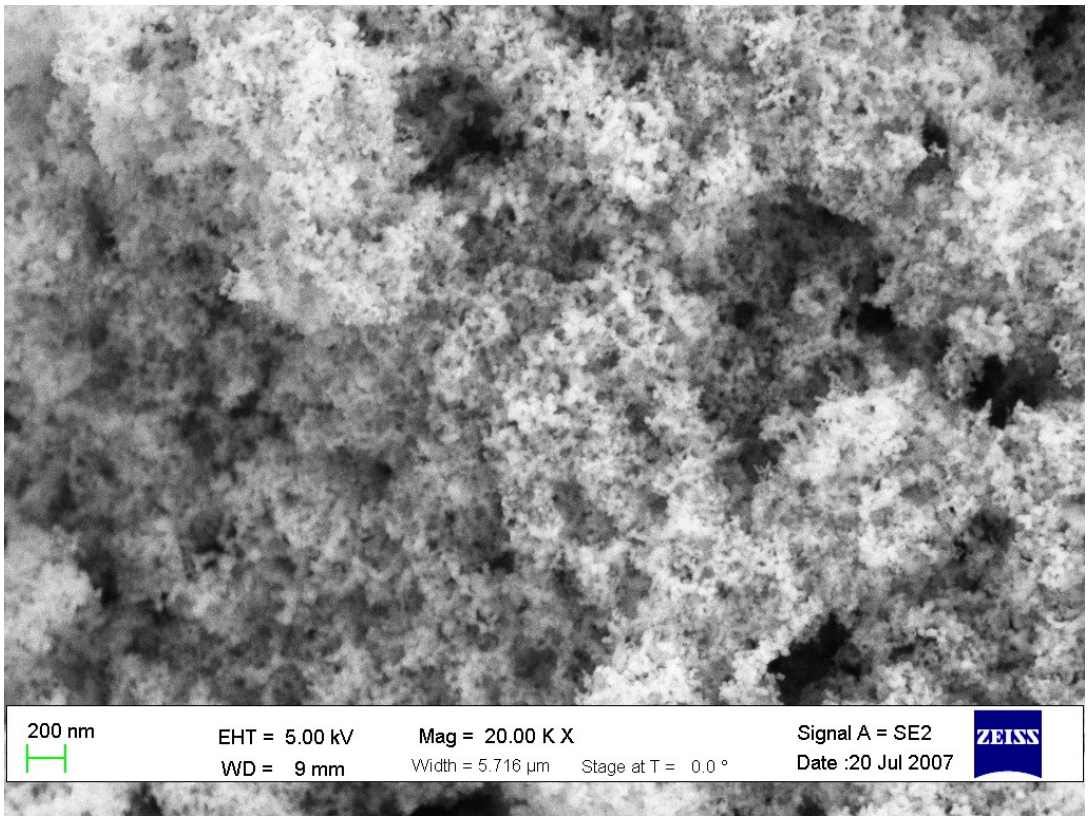

Figure 3.20. SEM image of the Degussa P-25 TiO_2 sample.

3.2.5 Photocatalytic Activity

Figures 3.21 and 3.22 show the change in concentration of $Cr(VI)$ with irradiation time during photocatalytic reaction using the $CS-TiO_2$ samples under visible light irradiation. The initial dose was 2g/L in all the cases and the initial concentration of $Cr(VI)$ was 800 μM at pH = 3.2. Data are shown for $CS-TiO_2$ samples derived from the two series of titanium oxide precursors, namely oxynitrate (Figure 3.21) and oxysulfate (Figure 3.22) along with those for the benchmark Degussa P-25 TiO_2 sample.

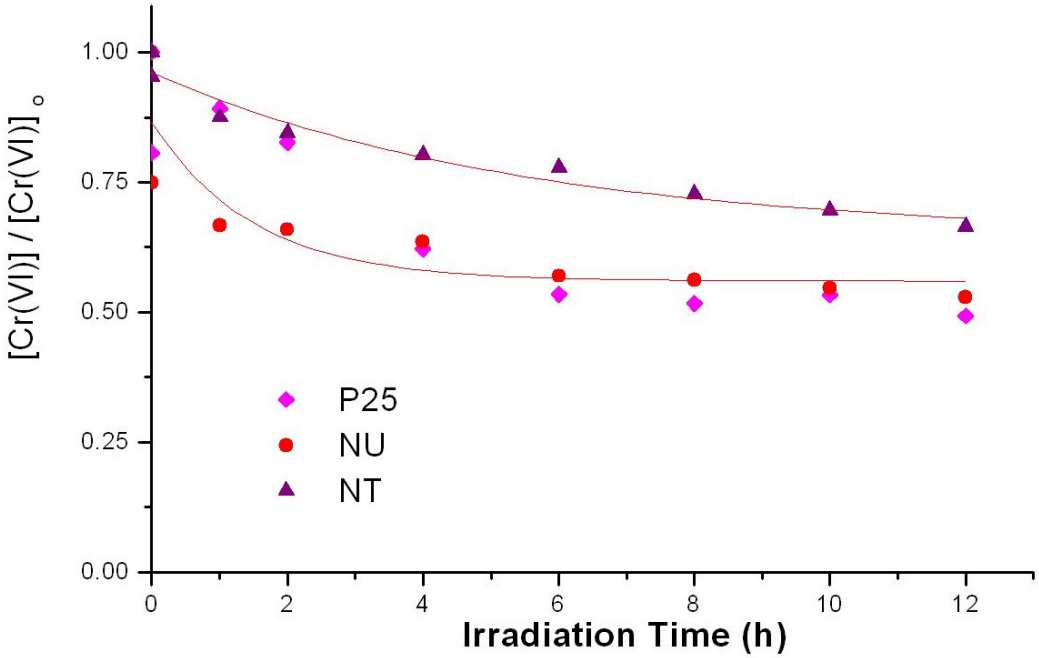

Figure 3.21. Visible light photocatalytic reduction profile of $Cr(VI)$ using $CS-TiO_2$ samples prepared from $TiO(NO_3)_2$ and different fuels as shown.

Remarkable differences can be seen for the two different series. As shown in Figure 3.21, no improvement in the photocatalytic performance toward reduction of $Cr(VI)$ was found for the as-prepared samples using nitrate salts when compared to commercial

Degussa P-25. Furthermore, the photocatalytic activity with the urea product (NU) aproached that of the reference P-25, while the use of thiourea (NT) even decrease the photocatalytic activity.

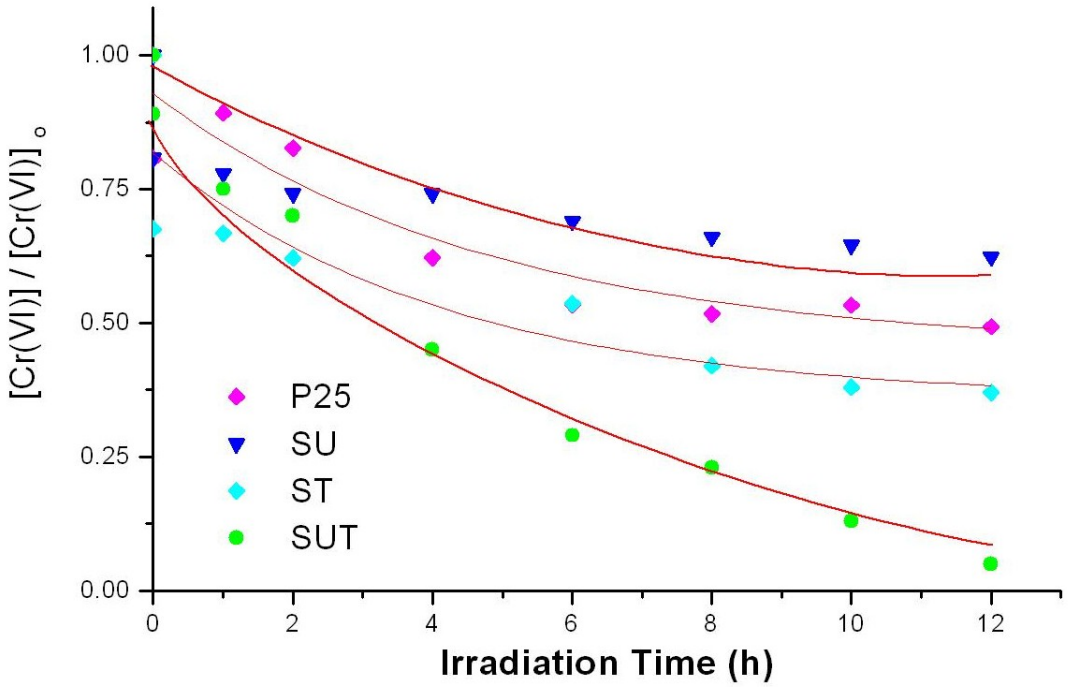

Figure 3.22. Visible light photocatalytic reduction profile of $Cr(VI)$ using $CS - TiO_2$ samples prepared from $TiOSO_4$ and different fuels as shown.

In contrast, $Cr(VI)$ reduction rates were found to be improved for the titanium oxysulfate salt and thiourea fuel (ST) when compared to the commercial sample (Figure 3.22). More interesting is the improvement when a mixture of the fuel was used (SUT); in this case, the final concentration of of $Cr(VI)$ after 12 hours of visible irradiation was close to zero. the use of urea (SU sample) did not improve the photocatalytic activity toward the reduction of $Cr(VI)$ under visible light irradiation.

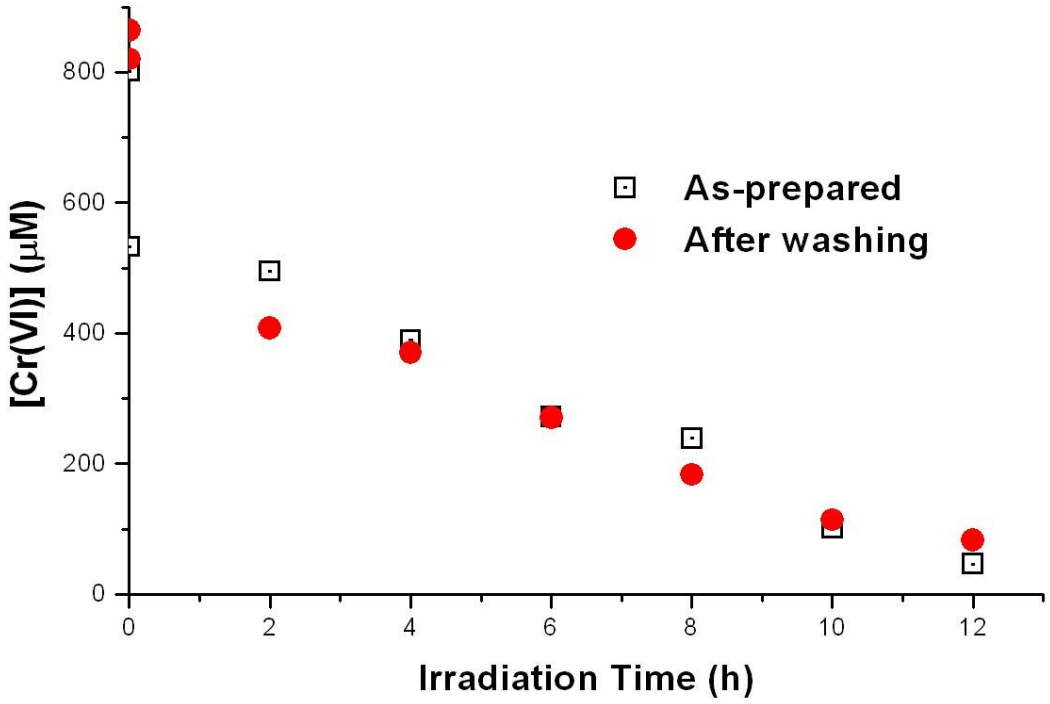

Figure 3.23. Photocatalyc activity of the SUT sample as prepared and washed.

To evaluate the effect of washing on the photocatalytic activity, the SUT sample was washed several times with deionized water, then dried in the oven overnight and used in the photocatalytic reduction of $Cr(VI)$. As can be seen in the $Cr(VI)$ concentration curves with respect to time under visible light (Figure 3.23) no appreciable change in the reduction rate was found between the as-prepared and washed samples.

The effect of annealing on the photocatalytic activity of the SUT sample was verified, Figure 3.24 shows the $Cr(VI)$ concentration curves with respect to time under visible light irradiation for as-prepared and annealed samples at 150 ^oC, 200 ^oC and 400^oC for 30 minutes. A decrease in photocatalytic activity can be seen with an increase in annealing temperature. Initially no appreciable change can be seen after heating at 150^oC or even 250^oC, but low photocatalytic activity is observed after heating at 400^oC.

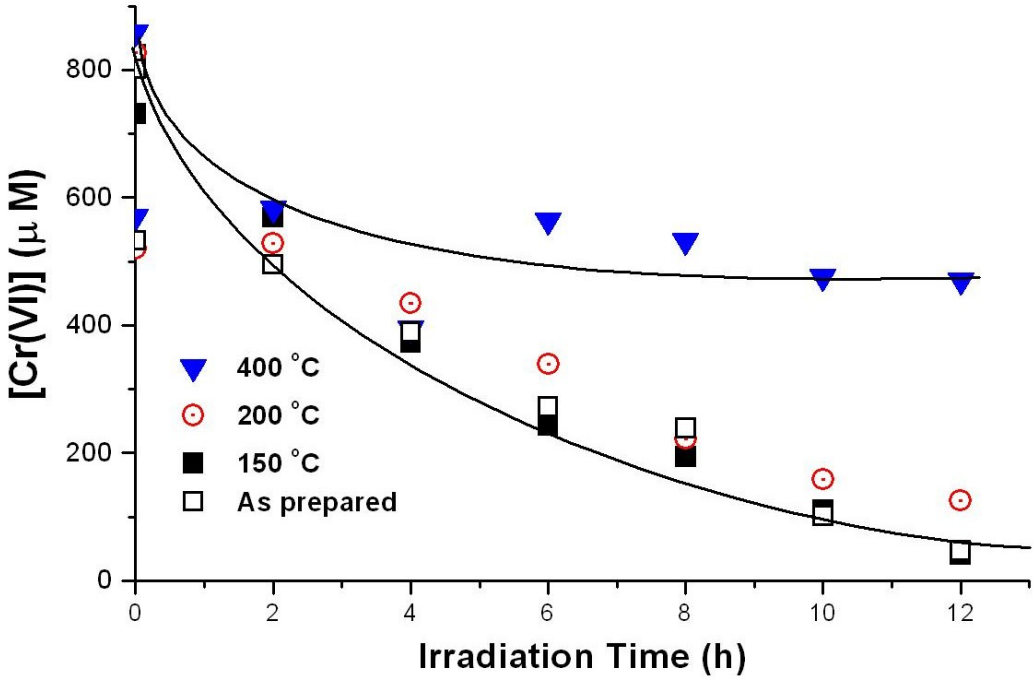

Figure 3.24. Effect of annealing on the photocatalytic activity of the SUT sample for $Cr(VI)$ reduction.

This is presumably a morphological consequence of thermal annealing; i.e., the surface area probably diminishes as a result of sintering.

3.3 Metal Co-doping

To evaluate if co-doping with metal ions is viable using the combustion synthesis technique, a set of reactions was carried out using a soluble salt containing an appropriate metal ion. Molybdenum was chosen for this purpose in the form of chloride ($MoCl_5$), due to the similar ionic radii of Mo and Ti, solubility of the chloride salt and also because higher valence cations such Mo^{5+} are expected to minimize recombination of the photogenerated charge carriers [30]. Three sets of samples were prepared, in each case 5% by weight of molybdenum chloride, titanium oxysulfate salt and urea ($SU+Mo$), thiourea ($ST+Mo$) or the mixture of fuels ($SUT+Mo$) were employed.

Figure 3.25. Physical appearance of samples prepared with the use of $MoCl_5$.

Each reaction was set up as described in experimental section for the oxysulfate series (section 2.2), with the only difference that 5% by mass of $MoCl_5$ was added to the initial mixture. The equivalent ratio was kept equal to unity in each case as before [56]. The final product obtained was a dry, foamy, brown solid (see Figure 3.25).

3.3.1 Diffuse Reflectance Spectroscopy

UV-vis transmittance spectra for the SUT samples prepared with the addition of molybdenum chloride salt show the absorption edge to be at longer wavelengths than that of the Degussa P-25 sample or the previous $CS - TiO_2$ samples. This can be seen in Figure 3.27, where the Tauc plots show a decrease in the band gap edge for the new $CS - TiO_2$ samples. Further analyses show that multiple band gap values can be extrapolated, obtaining three values in each case (see the case of $SUT + Mo$ in Figure 3.27). The first of these values was observed in the different samples with approximately the same energy (around 3.2 eV) while the two additional values were establish to be at different positions. These values are presented in Table 3.8 and show a narrowing effect

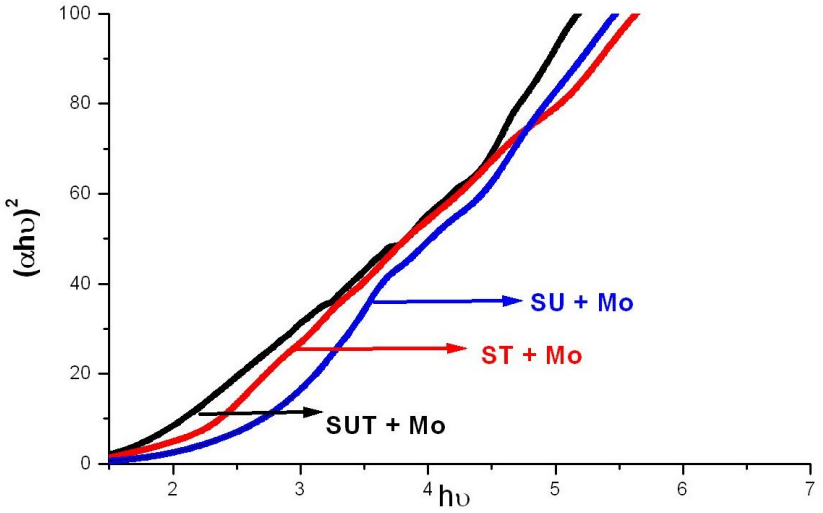

Figure 3.26. Tauc plots obtained for samples prepared using the oxysulfate series and 5.0% $MoCl_5$.

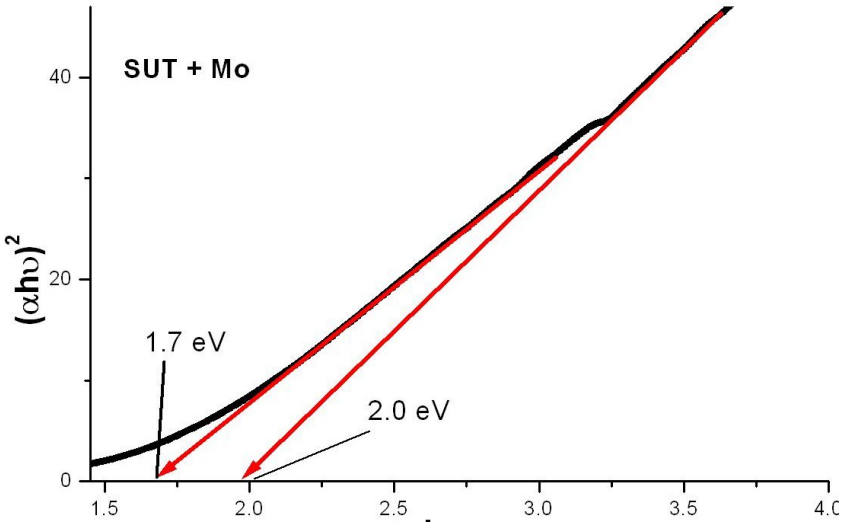

Figure 3.27. Tauc plot for the $SUT + Mo$ combustion synthesized sample. A third band gap value ($\approx 3.2\, eV$) is not shown for clarity.

Table 3.8. Band gap values for the different $CS-TiO_2$ samples made with the addition of 5.0% $MoCl_5$

Sample	E_g (eV)
SU	2.6
	3.1
	3.2
ST	2.0
	2.2
	3.2
SUT	1.7
	2.0
	3.2

on the optical band gap for each sample, in each case lower than that of Degussa P-25 (3.3 eV) or the samples obtained in the initial reaction (2.5 eV) (see section 3.3.1). The new band gaps energy are remarkably low (1.7 and 2.0 eV) for the sample that makes use of the mixture of fuels (see also Figure 3.27).

3.3.2 XPS

Samples were prepared using the new $CS-TiO_2$ samples and XPS spectra recorded. The photoelectron peak of $Ti\,2p$ core level did not show any change either in position or composition when compared to the initial system (without the use of $MoCl_5$).

The $O\,1s$ core level was recorded for the different samples, with the information obtained summarized as follows:

1. All samples show a broad peak that can be deconvoluted to three components showing no change in position relative to those obtained with the original mixture (*SUT*, *ST* or *SU*).

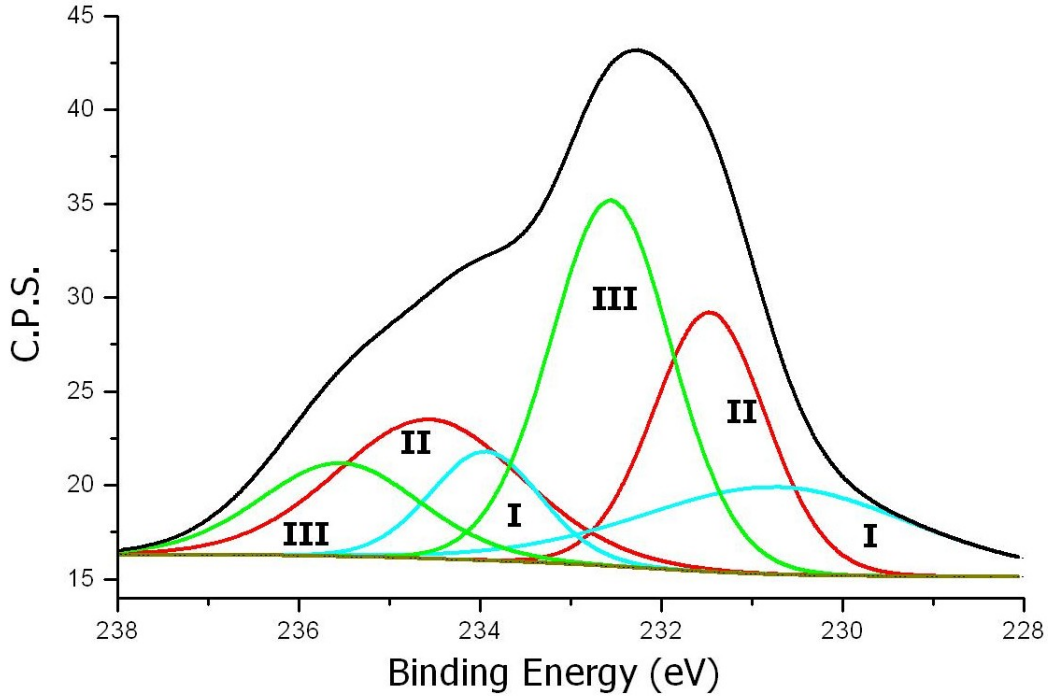

Figure 3.28. High resolution XPS spectra of $Mo\,3d$ core level for the $SUT + Mo$ sample showing the different contributions (see text for notation of components).

2. The main components for the $SUT + Mo$ and $ST + Mo$ samples were assigned to $Ti - O$ in the lattice and OH^- surface hydroxyl groups, just like in the original series.

3. In the case of the $SU + Mo$ sample, a high area around 532.5 eV was found as the main component for the $O\,1s$, this peak is assigned to the presence of $O - S$.

Deconvolution of the sulfur peak ($S\,2p$ core level) shows the presence of S^{6+} and S^{4+} (around 169.5 and 168.5 eV respectively). Just like in the original oxysulfate series the peak area related to S^{4+} was higher than the S^{6+} area in the case of thiourea and mixture of urea and thiourea fuels. For the $SU + Mo$ sample the ratio was higher in the S^{6+} species. No peaks associated with the formation of MoS_2 or TiS_2 were found, binding energies of these metal sulfur bond normally appear in the range 161-163 eV [86].

Table 3.9. $Mo\,3d$ binding energies (eV) in the $SUT + Mo$ sample

Curve	Oxidation state	Binding Energy (eV)	Area
A	$Mo(IV)$	230.8	17.9
		233.9	9
B	$Mo(V)$	231.5	22.1
		234.6	19.5
C	$Mo(VI)$	232.5	33.5
		235.5	11.2

The $Mo\,3d$ core level for the different samples shows a broad peak with a complex structure, that after deconvolution reveals spin-orbit splitting for the different oxidation states with a typical value of 3.2 eV ($\Delta BE = Mo3d_{5/2} - Mo3d_{3/2}$) [74]. Distinctive values for the different oxidation states of molybdenum were found for the different samples and the values for the $SUT + Mo$ sample are reported in Table 3.9. Figure 3.28 shows the curve fitting for the $SUT + Mo$ sample, where I represents molybdenum in oxidation state IV (as in MoO_2). II is the $Mo(V)$ oxidation state and III represents $Mo(VI)$ (like in MoO_3) [30, 74]. $Mo(0)$ has a binding energy around 228-229 eV and was not present in this particular sample [30, 74, 87, 88].

In summary, co-doping with Mo is possible as the radius of Mo^{6+} is close to that of Ti^{4+} (62 and 68 pm) [89]; thus it is likely that Mo ions could enter into the TiO_2 lattice displacing Ti^{4+}. The presence of the different oxidation states for molybdenum in the different $CS - TiO_2$ samples helps to confirm co-doping of the metal oxide. These values are in agreement with information previously reported using other synthesis methods [30, 88]. In sum, these XPS data show co-doping of the metal oxide host by sulfur (mainly S^{4+}) and molybdenum (mainly 6+, but also present as 4+ and 5+).

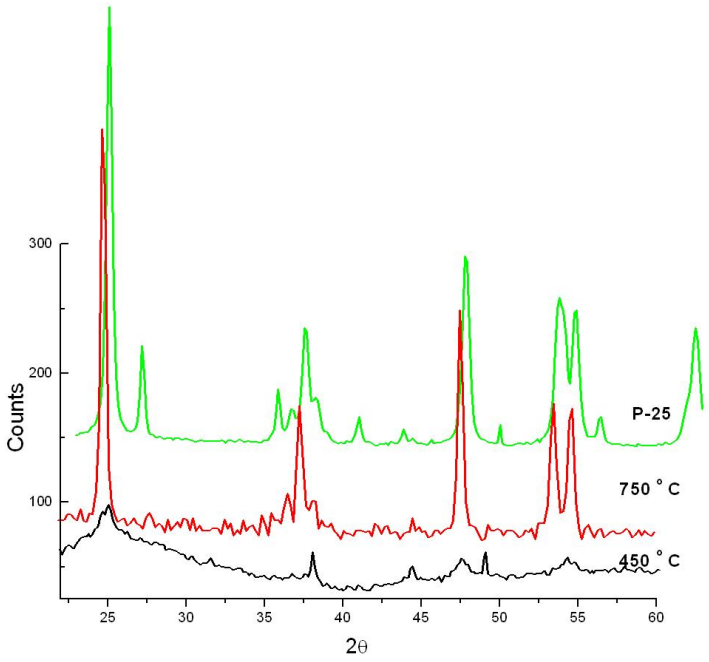

Figure 3.29. XRD of $SUT + Mo$ sample compared to the Degussa P-25 sample.

3.3.3 XRD

Figure 3.29 shows XRD spectra of a $CS - TiO_2$ sample prepared with the use of 5% $MoCl_5$ and annealed at 450 ^oC and 750 ^oC for 30 minutes. The crystalline size using the (101) peak after annealing at 450 ^oC and the Debye-Scherrer equation (see section 3.1) was calculated to be 9.37 nm. This increase in size is confirmed by the shape of the (101) peak for $SUT + Mo$ when compared to ST and SUT, as can be seen in Figure 3.30.

High resolution analysis of the (101) signal of the $SUT+Mo$, ST and SUT samples annealed at 450^oC shows a shift in the position of the (101) signal (see Figure 3.30). This again could be related to lattice distortion in the co-doped samples. Further analysis of these peak shifts is required and this work is in progress.

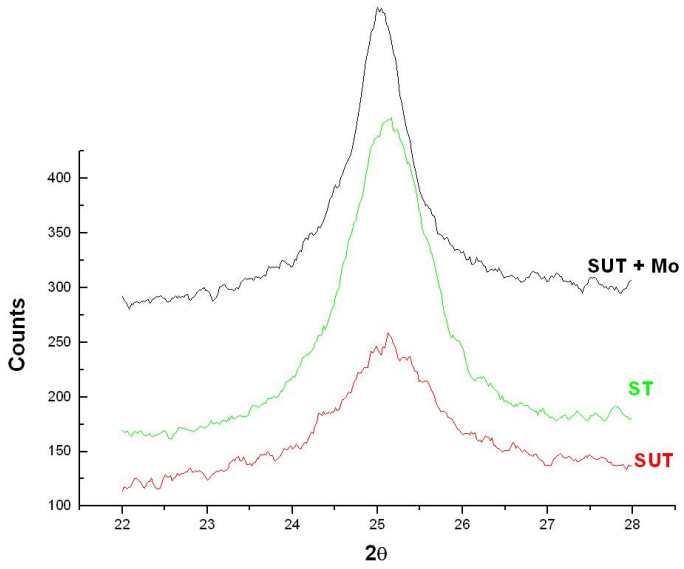

Figure 3.30. High resolution X-ray diffractograms of the (101) peak for SUT, ST and $SUT + Mo\ CS - TiO_2$ samples.

3.3.4 Photocatalytic Activity

Figure 3.31 shows the profile for the photocatalytic reduction of $Cr(VI)$ with the new samples prepared using the oxysulfate salt, different fuels and 5.0% by mass of $MoCl_5$. The Degussa P-25 and SUT samples are shown in the figure for comparison. The initial conditions were the same as those used in the original oxysulfate series. From this figure it is clear that photocatalytic activity was improved for the SUT and ST samples. Almost complete conversion of Cr(VI) is seen in a period of 4 to 5 hours under visible illumination (see Figure 3.31). The improvement can be visualized easily following Figure 3.32, where the remaining concentration of $Cr(VI)$ after four hours of visible irradiation is compared for different $CS - TiO_2$ samples. This represents an improvement in the overall photocatalytic activity of the new samples when compared to the initial $CS - TiO_2$ series or to the reference (Degussa P-25) TiO_2 sample.

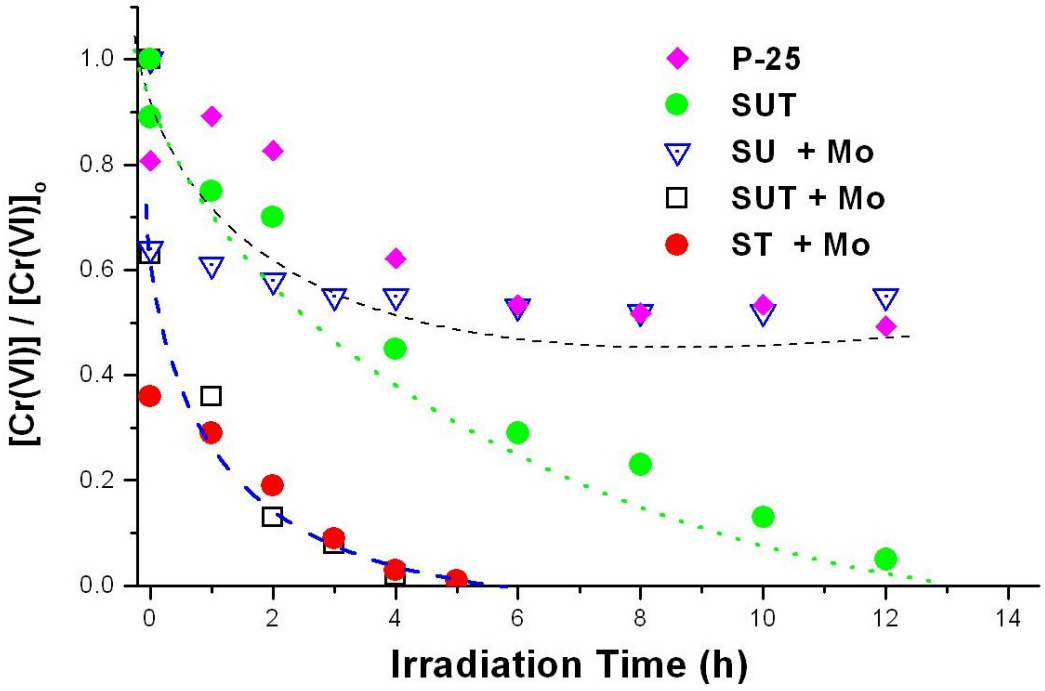

Figure 3.31. Photocatalytic activity of the co-doped $CS - TiO_2$ under visible light.

The effect of Mo co-doping on the photocatalytic activity can be understood as follows. The photocarriers generated by visible light separate with electrons being transferred to molecular oxygen producing a superoxide anion radical, and the holes produce hydroxyl radicals. Before recombination takes place, trapping of these charges is necessary to ensure photocatalytic activity. Higher valence electrons such as Mo^{5+} can replace Ti^{4+}, leaving extra holes weakly bound to the dopant center contributing to the conduction band. Then, electrons in the conduction band (e^-_{CB}) are trapped by the co-doped metal before recombination takes place, providing more electrons in the conduction band for the reduction of electron acceptor species [30]. As a result of the decrease of carrier recombination more super oxide radicals $O_2^{-\bullet}$ are also produced [30]. In the case of molybdenum it has been shown that Mo^{5+} and Mo^{6+} can co-exist simultaneously during illumination [87].

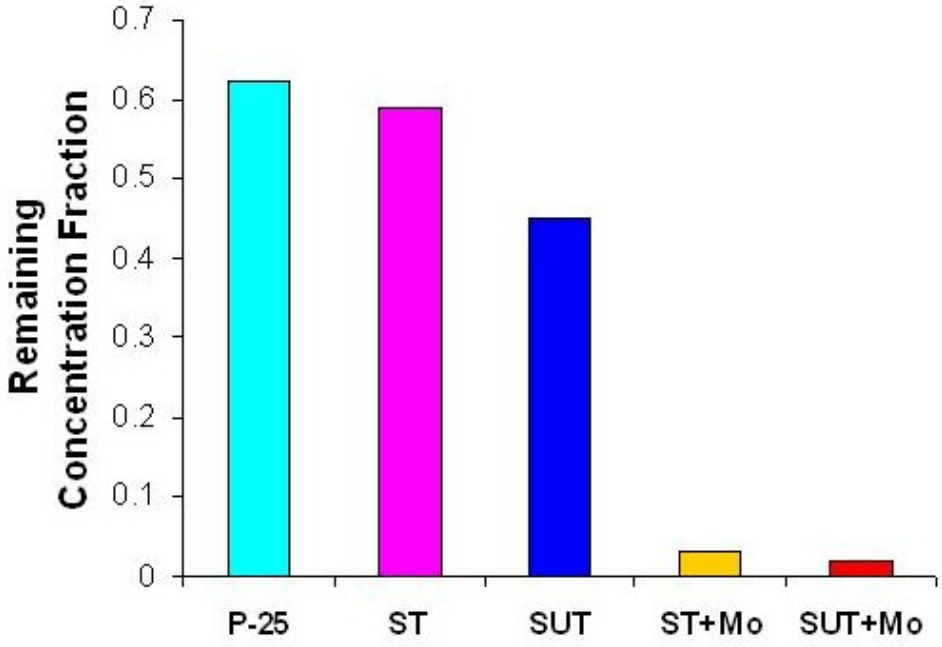

Figure 3.32. Photocatalytic activity of the various $CS - TiO_2$ samples for $Cr(VI)$ reduction after four hours of visible light irradiation.

CHAPTER 4

SUMMARY AND CONCLUDING REMARKS

This thesis research has shown that combustion synthesis is a simple, one step, low energy, easy method to prepare and improve titanium dioxide (TiO_2). All the $CS-TiO_2$ samples show a shift in absorption of light to higher wavelengths. The improvement in the absorption of light was obtained with the use of oxysulfate salt as oxidant and thiourea or mixtures in one to one ratio of urea and thiourea; the band gap values were found to be equal to 2.5 eV in the cases where thiourea or the mixture of fuels were used. These samples show dramatic improvement in the photocatalytic activity toward the reduction of $Cr(VI)$ under visible illumination. XPS studies show the presence of sulfur as dopant in these $CS-TiO_2$ samples as S^{+4} and S^{+6} species, along with high presence of hydroxyl groups adsorbed at the surface of the metal oxide. XRD proved the final oxide composition to be anatase and no noticeable conversion to rutile was found even after annealing to 750 ^oC.

Even though previous works did not find metallic co-doping of titania using this method, co-doping by molybdenum was demonstrated in this research. These new co-doped TiO_2 samples showed a significant rate of reduction of $Cr(VI)$ under visible irradiation. Two low band gaps were observed in the Tauc plots for this co-doped product making use of thiourea ($ST+Mo$) and the mixture of fuels ($SUT+Mo$); the values were 2.0 - 2.2 and 1.7 - 2.0 eV respectively. XPS studies found the molybdenum to be present as a mixture of oxidation states (mainly +6, but also as +4 and +3).

Neither carbon nor nitrogen doping was noted based on the XPS results. Substitution of sulfur for titanium in the structure of TiO_2 was also not observed. Further

studies are required to establish the mechanistic reasons for why thiourea (or mixtures with urea) yield superior TiO_2 samples relative to the use of urea alone as the fuel.

REFERENCES

[1] A. L. Linsebigler, G. Lu, and J. T. Yates Jr., *Chem. Rev.*, vol. 95, p. 735, 1995.

[2] J. M. Herrmann, *Catal. Today*, vol. 53, p. 115, 1999.

[3] M. R. Hoffmann, S. T. Martin, W. Choi, and D. W. Bahnemann, *Chem. Rev.*, vol. 95, p. 69, 1995.

[4] M. A. Fox and M. T. Dulay, *Chem. Rev.*, vol. 93, p. 341, 1993.

[5] A. Hagfeldt and M. Grätzel, *Chem. Rev.*, vol. 95, p. 49, 1995.

[6] K. Rajeshwar, *J. Appl. Electrochem.*, vol. 25, p. 1067, 1995.

[7] A. G. Agrios and P. Pichat, *J. Appl. Electrochem.*, vol. 35, p. 655, 2005.

[8] A. Sclafani, M. N. Mozzanega, and P. Pichat, *J. Photochem. Photobiol., A*, vol. 59, p. 181, 1991.

[9] A. Fujishima and K. Honda, *Nature,*, vol. 37, p. 238, 1972.

[10] T. L. Thompson and J. T. Yates Jr., *Chem. Rev.*, vol. 106, p. 4428, 2006.

[11] M. Grätzel, *Nature*, vol. 414, p. 338, 2001.

[12] U. Dieböld, *Surf. Sci. Rep.*, vol. 48, p. 53, 2003.

[13] H. Tributsch, *Coord. Chem. Rev.*, vol. 248, p. 1511, 2004.

[14] R. Asahi, T. Morikawa, T. Ohwaki, K. Aoki, and Y. Taga, *Science*, vol. 293, p. 269, 2001.

[15] C. D. Valentin, G. Pacchioni, and A. Selloni, *Phys. Rev. B*, vol. 70, p. 085116, 2004.

[16] R. Nakamura, T. Tanaka, and Y. Nakato, *J. Phys. Chem. B*, vol. 108, p. 10617, 2004.

[17] M. Miyauchi, A. Ikezawa, H. Tobimatsu, H. Irie, and K. Hashimoto, *Chem. Phys.*, vol. 6, p. 865, 2004.

[18] K. Kobayakawa, Y. Murakami, and Y. Sato, *J. Photochem. Photobiol. A*, vol. 170, p. 177, 2005.

[19] H. Wang and J. P. Lewis, *J. Phys.: Condens. Matter*, vol. 18, p. 421, 2006.

[20] C. D. Valentin, G. Pacchioni, and A. Selloni, *Chem. Mater.*, vol. 17, p. 6656, 2005.

[21] S. U. M. Khan, M. Al-Shahry, and W. B. Ingler, *Science*, vol. 297, p. 2243, 2002.

[22] T. Umebayashi, T. Yamaki, H. Itoh, and K. Asai, *Appl. Phys. Lett.*, vol. 81, p. 454, 2002.

[23] T. Umebayashi, T. Yamaki, S. Yamamoto, A. Miyashita, S. Tanaka, and K. A. T. Sumita, *J. Appl. Phys*, vol. 93, p. 5156, 2003.

[24] Z. Zhou, X. Zhang, Z. Wu, and L. Dong, *Chin. Sci. Bull.*, vol. 23, p. 2691, 2005.

[25] T. Ohno, T. Mitsui, and M. Matsumura, *Chem. Lett.*, vol. 32, p. 364, 2003.

[26] T. Ohno, M. Akiyoshi, T. Umebayashi, K. Asai, T. Mitsui, and M. Matsumura, *Appl. Catal., A*, vol. 265, p. 115, 2004.

[27] K. E. Karakitsou and X. E. Verykious, *J. Phys Chem.*, vol. 97, p. 1184, 1993.

[28] W. Mu, J. M. Herrmann, and P. Pichat, *Catal. Lett.*, vol. 3, p. 73, 1989.

[29] W. Y. Choi, A. Termin, and M. R. Hoffmann, *J. Phys. Chem.*, vol. 98, p. 13669, 1994.

[30] S. E. Park, H. Joo, and J. W. Kang, *Sol. Energy Mater. Sol. Cells*, vol. 83, p. 39, 2004.

[31] S. Karvinen, P. Hirva, and T. A. Pakkanen, *THEOCHEM Journal of Molecular Structure*, vol. 626, p. 271, 2003.

[32] K. Wilke and H. D. Breuer, *J. Photochem. Photobiol., A*, vol. 121, p. 49, 1999.

[33] C. N. R. Rao, *Mater. Sci. Eng., B*, vol. 18, p. 1, 1993.

[34] E. Santacesaria, M. Tonello, G. Storti, R. C. Pace, and S. Carra, *J. Colloid Interface Sci*, vol. 111, p. 44, 1986.

[35] Y. Kera, H. Kominami, S. Murakami, and B. Ohtani, *Photocatalysis: Science and Technology*, M. Kaneko and I. Okura, Eds. New York: Springer, 2002.

[36] C. Natarajan and G. Nogami, *J. Electrochem. Soc.*, vol. 143, p. 1547, 1996.

[37] N. R. de Tacconi, C. R. Chenthamarakshan, G. Yogeeswaran, A. Watcharenwong, R. S. de Zoysa, N. A. Basit, and K. Rajeshwar, *J. Phys. Chem. B*, vol. 110, p. 25347, 2006.

[38] M. Takeuchi, H. Yamashita, M. Matsuoka, M. Anpo, T. Hirao, N. Itoh, and N. Iwamoto, *Catal. Lett.*, vol. 66, p. 185, 2000.

[39] C. D. Tewillinger and Y. M. Chiang, *Nanostruct. Mater.*, vol. 2, p. 37, 1993.

[40] M. K. Akhtar, S. E. Pratsinis, and S. V. R. Mastrangelo, *J. Am. Ceram. Soc.*, vol. 75, p. 3408, 1992.

[41] J. Rubio, J. L. Oteo, M. Villegas, and P. J. Duran, *Mater. Sci.*, vol. 32, p. 643, 1997.

[42] S. J. Kim, D. Hwang, N. Lee, S. Shin, and S. J. Kim, *Jpn. J. Appl. Phys., Part 1*, vol. 44, p. 7703, 2005.

[43] M. Schneider and A. Baiker, *J. Mater. Chem.*, vol. 2, p. 587, 1992.

[44] P. Billik and G. Plesch, *Mater. Lett.*, vol. 61, p. 1183, 2007.

[45] T. Masui, K. Fujiwara, K. Machida, and G. Adachi, *Chem. Mater.*, vol. 10, p. 2197, 1997.

[46] E. Stathatos, P. Lianos, F. D. Monte, D. Levy, and D. Tsiourvas, *Langmuir*, vol. 1997, p. 4296, 13.

[47] Y. V. Kolenko, B. R. Churagulov, M. Kunst, L. Mazerolles, and C. Colbeau-Justin, *Appl. Catal., B*, vol. 54, p. 51, 2004.

[48] K. C. Patil and S. T. Aruna, *Redox Methods in SHS Practice*, A. A. Borisov, L. DeLuca, and A. Merzhanov, Eds. New York: Taylor and Francis, 2002.

[49] C. M. Wang, H. Wu, and S. L. Chung, *J. Poruous Mater.*, vol. 13, p. 307, 2006.

[50] S. Yamabi and H. Imai, *Thin Solid Films*, vol. 434, p. 86, 2003.

[51] A. A. Borisov, L. DeLuca, and A. Merzhanov, Eds., *Self-Propagating High-Temperature Synthesis of Materials.* New York: Taylor and Francis, 2002.

[52] A. Varma, *Sci. Amer.*, vol. 283, p. 44, 2000.

[53] K. Nagaveni, M. S. Hegde, N. Ravishankar, G. N. Subbanna, and G. Madras, *Langmuir*, vol. 20, p. 2900, 2004.

[54] K. C. Patil, S. T. Aruna, and S. Ekambaram, *Curr. Opinion in solid state and Mater. Sci.*, vol. 2, p. 158, 1997.

[55] K. C. Patil, *Bull. Mater. Sci.*, vol. 16, p. 533, 1993.

[56] S. R. Jain, K. C. Adiga, and V. R. P. Verneker, *Combust. Flame*, vol. 40, p. 71, 1981.

[57] S. T. Aruna and K. C. Patil, *J. Mater. Synth. Process.*, vol. 4, p. 175, 1996.

[58] G. Yogeeswaran, C. R. Chenthamarakshan, N. R. de Tacconi, and K. Rajeshwar, *J. Mater. Res.*, vol. 21, p. 3234, 2006.

[59] M. S. Hedge, K. Nagaveni, and S. Roy, *Pramana - J. Phys*, vol. 65, p. 641, 2005.

[60] K. Nagaveni, G. Sivalingam, M. S. Hegde, and G. Madras, *Appl. Catal., B*, vol. 48, p. 83, 2004.

[61] S. P. Vijayalakshmi and G. Madras, *J. Appl. Polym. Sci.*, vol. 100, p. 3997, 2006.

[62] G. Sivalingam and G. Madras, *Appl. Catal., A*, vol. 269, p. 81, 2004.

[63] G. Sivalingam, M. S. Hegde, and G. Madras, *Appl. Catal., A*, vol. 45, p. 23, 2003.

[64] C. H. Jung, J. Y. Park, S. J. Oh, H. K. Park, Y. S. Kim, D. K. Kim, and J. H. Kim, *J. Nucl. Mater.*, vol. 245, p. 203, 1998.

[65] D. V. Kimbrough, Y. Cohen, A. M. Winer, L. Creelman, and C. Mabuni, *Environ. Sci. Technol.*, vol. 29, p. 1, 1999.

[66] S. Pamukcu, A. Weeks, and J. K. Wittle, *Environ. Sci. Technol.*, vol. 38, p. 1236, 2004.

[67] S. J. Hug, H. Laubsher, and B. R. Jame, *Environ. Sci. Technol*, vol. 31, p. 160, 1997.

[68] C. R. Chenthmarakshan, K. Rajeshwar, and E. J. Wolfrum, *Langmuir*, vol. 16, p. 2715, 2000.

[69] W. Y. Lin, C. Wei, and K. Rajeshwar, *J. Electrochem. Soc.*, vol. 140, p. 2477, 1993.

[70] D. Harris, *Quantitative Chemical Analysis*. New York: W.H. Freeman Company, 2003.

[71] K. Rajeshwar, C. R. Chenthamarakshan, Y. Ming, and W. J. Sun, *J. Electroanal. Chem.*, vol. 173, p. 538, 2002.

[72] J. I. Pankove, *Optical Processes in Semiconductors*. Englewood Cliffs, NJ: Prentice Hall, 1971.

[73] G. Balasubramanian, D. D. Dionysiou, and M. T. Suidan, "Titanium dioxide coating on stainless steel," *Encyclopedia of Nanoscience and Nanotechnology*, 2004.

[74] C. D. Wagner, W. M. Riggs, L. E. Davis, and J. F. Moulder, *Handbook of X-Ray Photoelectron Spectroscopy*. Minnesota: Eden Prairie, Perkin Elmer Corporation, 1979.

[75] H. Sun, Y. Bai, Y. Cheng, W. Jin, and N. Xu, *Ind. Eng. Chem. Res.*, vol. 45, p. 4971, 2006.

[76] S. K. Prokes, J. L. Gole, X. Chen, C. Burda, and E. Carlos, *Adv. Funct. Mater.*, vol. 15, p. 161, 2005.

[77] D. Gonbeau, C. Guimon, G. Pfister-Guillouzo, A. Levasseur, G. Meunier, and R. Dormoy, *Surf. Sci.*, vol. 254, p. 81, 1991.

[78] D. Morris, Y. Dou, J. Rebane, C. E. J. Mitchell, and R. G. Egdell, *Phys. Rev. B*, vol. 61, p. 13445, 2000.

[79] B. M. Gatehouse, S. N. Platts, and T. B. Williams, *Acta Crys. B*, vol. 49, p. 428, 1993.

[80] M. Wahlqvist and A. Shchukarev, *J. Electron. Spectrosc. Relat. Phenom.*, vol. 156, p. 310, 2007.

[81] D. I. Sayago, P. Serrano, O. Bohme, G. Paolucci, E. Roman, and J. A. Martin-Gago, *Phys. Rev. B*, vol. 64, p. 205402, 2001.

[82] E. L. D. Hebenstreit, W. Hebenstreit, and U. Diebold, *Surf. Sci.*, vol. 461, p. 87, 2000.

[83] T. Ohno, T. Tsubota, Y. Nakamura, and K. Sayama, *Appl. Catal., A*, vol. 288, p. 2281, 2005.

[84] R. Bacsa, J. Kiwi, T. Ohno, P. Albers, and V. Nadtochenko, *J. Phys. Chem. B*, vol. 109, p. 5994, 2005.

[85] H. D. Jang, S. K. Kim, and S. J. Kim, *J. Nanopart. Res.*, vol. 3, p. 141, 2001.

[86] J. C. Dupin, D. Gonbeau, I. Martin-litas, P. Vinatier, and S. Levasseur, *Appl. Surf. Sci.*, vol. 173, p. 140, 2001.

[87] M. Grätzel and R. Howe, *J. Phys. Chem.*, vol. 94, p. 2566, 1990.

[88] N. V. Alov, *J. Anal. Chem.*, vol. 60, p. 431, 2005.

[89] J. E. Huheey, *Inorganic Chemistry: Principles of Structure and Reactivity.* New York: Harper Row, 1993.

BIOGRAPHICAL STATEMENT

Walter A. Morales Osorio was born in Medellin, Colombia. He received his B.S. Degree in Chemistry from The University of Antioquia, Medellin-Colombia, in 2001. He obtained his Masters Degree of Science in Chemistry from The University of Texas at Arlington in 2007.